We are IntechOpen,
the world's leading publisher of
Open Access books
Built by scientists, for scientists

6,900
Open access books available

185,000
International authors and editors

200M
Downloads

154
Countries delivered to

Our authors are among the

TOP 1%
most cited scientists

12.2%
Contributors from top 500 universities

CLARIVATE ANALYTICS
BOOK CITATION INDEX
INDEXED

WEB OF SCIENCE™

Selection of our books indexed in the Book Citation Index
in Web of Science™ Core Collection (BKCI)

Interested in publishing with us?
Contact book.department@intechopen.com

Design of a Ku Band Planner Receive Array for DBS Reception Systems

Mustafa Murat Bilgic and Korkut Yegin

Abstract

The main objective of this chapter is to present to the readers a step-by-step design approach when designing antenna array. Subsequently, the chapter will proceed following an example design of a passive Ku band planner receive array antenna for direct broadcast from satellite (DBS) reception for mobile systems. First, an appropriate antenna topology capable of reaching our target goals will be selected and optimized to be the base array element. During the design process of the base element, some figures-of-merit will be proposed in order to make a comparative study with the designed antenna and previously published antenna structures. Subarrays of microstrip line feed antennas will be combined by waveguides in order to build a low-loss feed network for the array antenna. The main question during the design of the feed network is: "How should one form the subarrays and their accompanying waveguide feed networks?" These sections will answer this question by formulating the subarray and array feed network loss as an optimization problem with constraints on the size and the weight of the array. In the concluding sections, measurements on realized antennas will show that the design exhibits a 16.5% relative bandwidth, covering the complete downlink band, and the designed antennas have a 28.4–31.3 dBi gain for both vertical and horizontal polarizations. Results of some field tests will be given and conclusions will be made in the final section.

Keywords: wideband antennas, antenna arrays, hybrid feed networks

1. Introduction

Antennas are crucial components needed during the design of systems in which information is transmitted via electromagnetic waves. Special attention must always be paid to the antenna design in order to build up an efficient system. Antenna engineering is the area in which

engineers are specialized in designing antennas for a wide range of applications. Each application may require a different approach during the design process; also in each approach, engineers will come across different challenges. Antenna engineering is a fascinating application of electromagnetic theory where theory and practice are collated to form a beautiful harmony.

One can find a vast number of fairly comprehensive books on antenna theory written by some of the greatest scholars. Each year an enormous number of academic papers are being published, expanding the area of antenna theory. However, very few resources on practical design procedures are available. The main objective of this chapter is to show a step-by-step design procedure for a large antenna array that will hopefully give valuable insight to young engineers who are at the beginning of their path to become an antenna engineer.

The text following this section will first define the antenna problem. The specifications that a planner Ku band receive antenna array must necessarily achieve for reception of direct broadcast from satellite (DBS) systems will be defined. Section 3 will cover the design of a high performance antenna array element. A suitable microstrip antenna topology will be selected based on some figures-of-merit that will be defined according to the given specifications. The selected structure will be optimized to supply the best performance and a comparative study between previously published examples will be executed. Section 4 will show the design of optimal subarrays and microstrip line feed networks. These subarrays will then be combined with waveguides to build up a larger array. Finally, measurement results of realized antennas will be discussed.

2. System level requirements for mobile satellite TV antennas

Information and entertainment systems for reception of direct broadcast from satellite (DBS) on mobile environments have been a great challenge for the automotive industry. Over the last two decades, there has been growing interest for developing low-cost, high performance systems working on mobile platforms. Such systems in automobiles now demand compact mobile antennas for reception of DBS from different service providers simultaneously.

Most of the existing commercial products were based on reflector-type antennas, which possess excellent bandwidth, gain, noise figure, and half power beam width (HPBW) characteristics. These aspects also make these antennas ideal candidates for control and tracking of satellites while the vehicle is on the move. Satellite tracking with reflector-type antennas is basically carried out by mechanically steering the antenna in both the elevation and the azimuth axes. However, the bulky size and high profile of reflector antennas cause aerodynamic problems on vehicles. Moreover, these structures are not suitable for smaller vehicles. A low profile structure such as microstrip antenna arrays with reduced size would be more advantageous. The primary specification is to build a planner structure using microstrip antennas which would hold the same properties of a reflector antenna. The low profile antenna would also be mechanically steered in both elevation and azimuth planes so that no active components such as phase shifters hence amplifiers would be necessary.

In the field of TV broadcasting, geostationary satellites are set apart 6° or more from each other: For azimuth tracking, the antenna's half power beam width is commonly preferred to be less than 5° whereas it is chosen to be more than 1.5° to optimize tracking the satellite on a moving vehicle. In order to successfully lock to the satellite over a 32 MHz IF bandwidth, which is the maximum bandwidth for TurkSat,[1] a minimum of 7 dB of carrier-to-noise ratio (CNR) is required.

It is possible to achieve high antenna gain throughout a maximum of 3° azimuth HPBW in a planar microstrip antenna array with appropriate number of elements. However, maintaining target antenna gain at low elevation angles is difficult with broadside antenna elements. The TM_{20} mode type radiation pattern may be more suitable, but achieving target bandwidth with such patch is extremely challenging. Besides, the antenna size would be much larger compared to TM_{01} mode broadside looking patch. Utilizing subarrays or panels, positioned on the same platform, which are capable of being mechanically tilted to certain elevation angles would be a compromise on height profile. Yet this still is a more expensive choice and it also complicates the control of the system. This solution is known to have been used in previous studies [1–5] and it is still broadly used in many satellite systems. Added complexity of this system out-weighs the benefits of fulfilling electrical specifications.

At this point, it will be suggested to use two panels built from microstrip patch antennas for each polarization to minimize the added complexity of this implementation. The array will be formed in order to have a tilted beam. Since the array can be mechanically tilted, it would be easier to scan low elevation angles without exceeding the overall height limits. The system configuration of the proposed design is illustrated in **Figure 1**.

The directivity of a TM_{01} mode broadside patch is roughly:

$$D_P = \frac{4\pi}{\Omega_A} \approx \frac{4\pi}{\pi} = 4(6 \text{ dBi}) \tag{1}$$

where, Ω_A represents beam solid area. For K elements, the array directivity D_A becomes:

$$D_A \approx K D_P \tag{2}$$

If elevation scanning of $\pm 15°$ is assumed, $HPBW_\theta$ in elevation can be taken as 30°. $HPBW_\varnothing$ can be set to 3° for azimuth tracking. Then, the directivity of the array is roughly [6]:

$$D_A \approx \frac{40,000}{HPBW_\theta HPBW_\varnothing} \approx 444(26.47 \text{ dBi}) \tag{3}$$

Furthermore, if 55% total efficiency (due to feed network loss, mismatch loss) is assumed, the gain of the array should be 807 (29 dBi). Number of broadside patch elements required for this gain is 202. To preserve symmetry and to account for other losses (e.g. random, mutual coupling among array elements), we estimate that 256 elements per polarization is needed.

---

[1]The antenna in this design example is for the transponders fixed on TurkSat 2A and 3A satellite. It is positioned to an elevation angle of 42°E in Turkey.
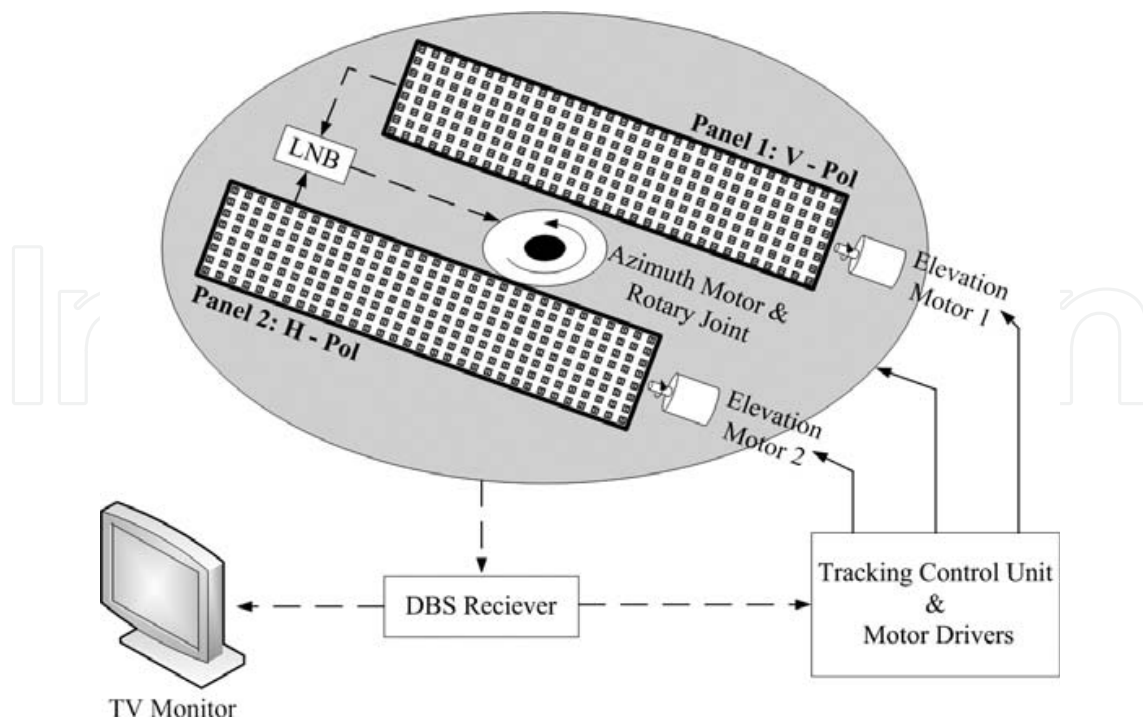
Figure 1. System configuration of the proposed array antenna.

Based on the simple calculations given above and a quick overview of some commercial products, the target system specifications are formed and summarized in **Table 1**.

Specification	Value
Frequency	10.8–12.8 GHz
Polarization	Dual linear (vertical and horizontal)
Antenna G/T (EIRP >54 dBW)	>5.5 dB/°K at 45° elevation
Antenna gain	29 dBi (per polarization)
Spatial coverage	35–75° elevation, 0–360° azimuth
Antenna height (w/max mechanical tilt)	<70 mm
System diameter	<75 cm
Weight (w/o electromechanical components)	<3 kg

Table 1. Target system specifications.

3. Wideband, high gain antenna element design

Based on the specifications given in Section 2, a high gain and wideband planar antenna is desired. When designing such antennas, the first step should be achieving the target bandwidth. Antenna gain becomes the next goal, because gain directly impacts signal-to-

noise ratio (SNR) of the system. Often, minimum gain in the target bandwidth is specified to fulfill SNR requirements. However, gain and bandwidth are usually complementary metrics where the improvement in one, results in the degradation of the other. Thus, one must optimize the design for gain-bandwidth product (GBWP) rather than bandwidth/gain only. An upper bound on gain-bandwidth product can be placed for electrically small antennas [7, 8], but this is rather difficult for multiple resonant or wideband antennas.

One of the most common planar antenna configurations is the aperture-coupled microstrip antenna (ACMSA) configuration [9]. Slot coupling is also suitable for high-frequency applications where structural dimensions are in millimeter or submillimeter range. Most of these applications need high directive gain; thus, utilize phased arrays where high gain and wideband antenna elements are required. To increase the bandwidth of an ACMSA, parasitic elements in the form of stacked patches or coplanar parasitic elements were proposed [10, 11]. Unlike coplanar parasitic elements, stacked patches do not increase the aperture area of the antenna, hence they do not require increased interelement spacing that may cause grating lobes. Either a nonresonant slot is coupled to stacked resonant patches or a resonant slot radiates with resonant stacked elements. Stacked patches coupled with a resonant slot exhibit fractional bandwidth (FBW) more than 50% with gain in excess of 5 dBi [12, 13]. For nonresonant slot coupling, various slot shapes ranging from rectangular slots to dog-bone shape slots have been proposed [9–15]. Hourglass shape nonresonant slot was identified as the best configuration in terms of fractional bandwidth [10]. However, none of these studies considered GBWP, and which configuration produces best gain-bandwidth performance is yet unknown. Also, it is still unclear whether resonant slot or nonresonant slot has better performance.

In any antenna design, bandwidth, gain, and HPBW are the most essential design characteristics along with other features such as cross polarization ratio, front-to-back ratio, in-band gain ripple, electrical height, and physical dimensions. Although it is difficult to define a common figure-of-merit (FOM) to combine all these metrics into one, several FOMs will be derived based on GBWP. Performance-wise comparisons of various nonresonant and resonant aperture coupled stacked patches will be defined for the best configuration in terms of these FOMs.

This design is particularly focused on Ku band applications for mobile satellite TV reception and satellite communications. A wideband equivalent circuit representation of the optimized ACMSA will be derived. Based on this study, a high gain, wideband antenna structure operating at Ku band with highest FOM compared to earlier studies will be proposed. Realized antenna and measurement results will also be provided.

3.1. Gain-bandwidth product of rectangular patch antenna

The bandwidth for a rectangular patch antenna with length L, width W and substrate height h is given as:

$$BW = \frac{VSWR-1}{Q\sqrt{VSWR}} \tag{4}$$

where, Q represents the quality factor of the patch. Fractional bandwidth rather than absolute bandwidth is regarded as the bandwidth, thus, BW can also be expressed as:

$$BW = \frac{f_u - f_l}{f_c} \tag{5}$$

where, f_u, f_l and f_c represent upper, lower, and center frequency of the impedance match frequency band.

For VSWR < 2, BW becomes:

$$BW = \frac{1}{Q\sqrt{2}} \tag{6}$$

For electrically thin substrates ($h/\lambda \ll 1$), BW can be estimated as [16]:

$$BW = \frac{16}{6\pi\sqrt{2}} \frac{c_1 p}{e_r} \frac{k_0 h}{\varepsilon_r} \frac{W}{L} \tag{7}$$

where, e_r is the efficiency, $k_0 = 2\pi/\lambda_0$ (free space wavenumber), ε_r is the permittivity of the substrate, c_1 and p are functions used in the approximation [17]. For $W/L < 2$, p becomes almost 1, and c_1 becomes 0.4 for air-dielectric and nearly 1 for high permittivity substrates. It is clear from Eq. (6) that the electrical height of the antenna is directly proportional to the bandwidth. For a given substrate height, the bandwidth is relatively wider at higher frequencies.

The gain of the patch antenna is approximated as [18]:

$$G = \frac{4(k_0 W)^2}{\pi \eta_0} e_r R_r \tag{8}$$

where, R_r represents radiation resistance. R_r given in Ref. [19] was not very accurate as stated by its authors so a more accurate representation given in [20] can be used. R_r given in [20] is approximated to its leading terms and is proportional to:

$$R_r = \varepsilon_r 1 \over (k_0 h)^2 (k_0 w/2)^2 \left[-1 + \frac{14}{(k_0 w/2)^2} \right] \tag{9}$$

The gain of the antenna is inversely proportional to $(k_0 h)^2$. Hence, neglecting the constants and assuming p equals to 1, GBWP for rectangular patch is proportional to:

$$GBWP = \frac{1}{k_0 h} \frac{W}{L} \frac{1}{\left[-1 + \frac{14}{(k_0 w/2)^2} \right]} \tag{10}$$

Therefore, increasing $k_0 h$ for bandwidth improvement deteriorates attainable gain and limits GBWP. High aspect ratio (W/L) also improves GBWP if higher order modes are not excited. It

is interesting to see that substrate permittivity and antenna efficiency are not the factors of GBWP. Low permittivity substrates are good for bandwidth improvement but relatively worse for antenna gain. Aperture-coupled antennas mostly follow the same trend of rectangular antennas, however, approximate relations are quite difficult to obtain.

Although these approximate formulas have been widely accepted, they are only valid for electrically thin substrates. 3D simulations were performed on rectangular patch antenna with pin feed and defined GBWP as:

$$\text{GBWP} = \frac{\int_{f_l}^{f_u} G(f)df}{f_u - f_l} \left(\frac{f_u - f_l}{f_c} \right) \tag{11}$$

where, $f_l \leq f_i \leq f_u$, $i = 1, 2,\ldots, N$ and $G(f)$ represents gain (linear not decibel) as a function of frequency. Rectangular patch antenna is optimized for best GBWP for different $k_0 h$ and substrates of different relative permittivity ε_r. The results are shown in **Figure 2**. Unlike approximate formulas, simulations show that GBWP has a maximum at certain $k_0 h$ and it is maximum for air-dielectric substrate. A similar analysis for different patch aspect ratios has also been simulated for air-dielectric patch only (see **Figure 3**). Again, it appears that there exists an optimum electrical height where GBWP is optimal. All simulations were run around Ku-band downlink frequency band (10.8–12.8 GHz).

GBWP performance has also been compared between pin-feed rectangular patch antenna and nonresonant rectangular slot coupled patch antenna, and the results are displayed in **Figure 4**. It can be observed that slot-coupled geometry produces much better GBWP performance as the inductance of pin feed severely limits BW of rectangular patch antenna.
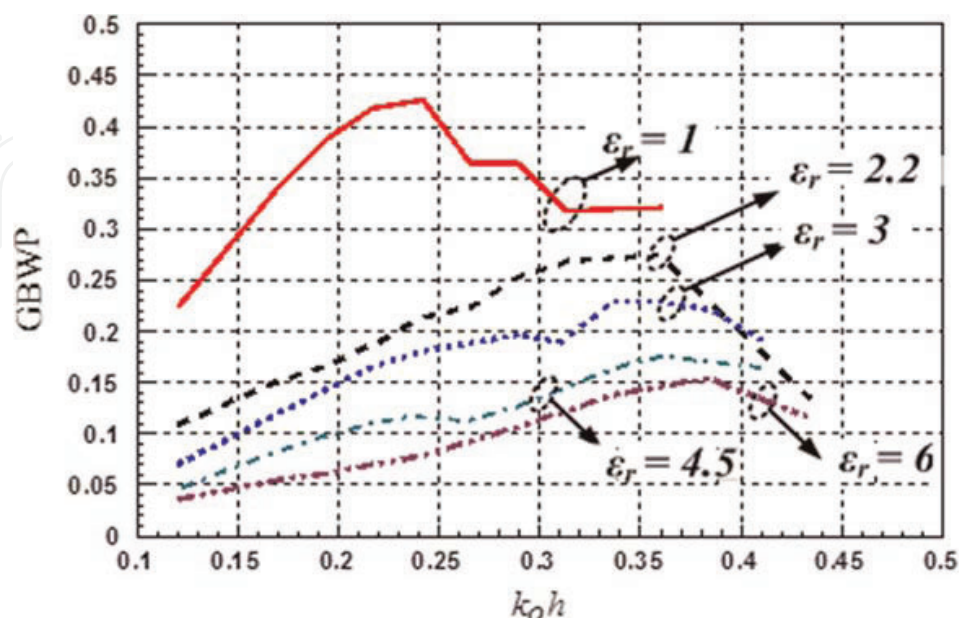

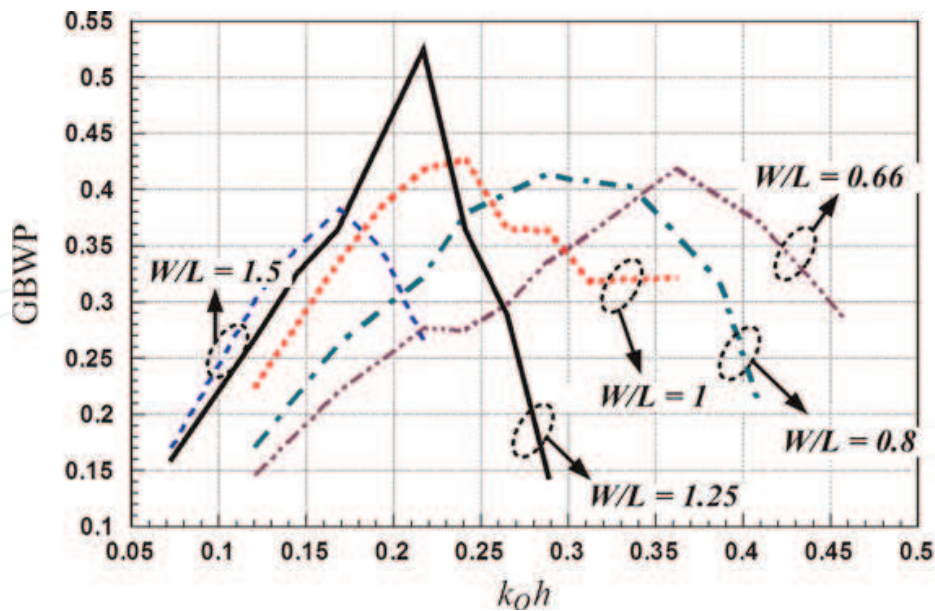**Figure 2.** GBWP vs. $k_0 h$. for different dielectric materials.

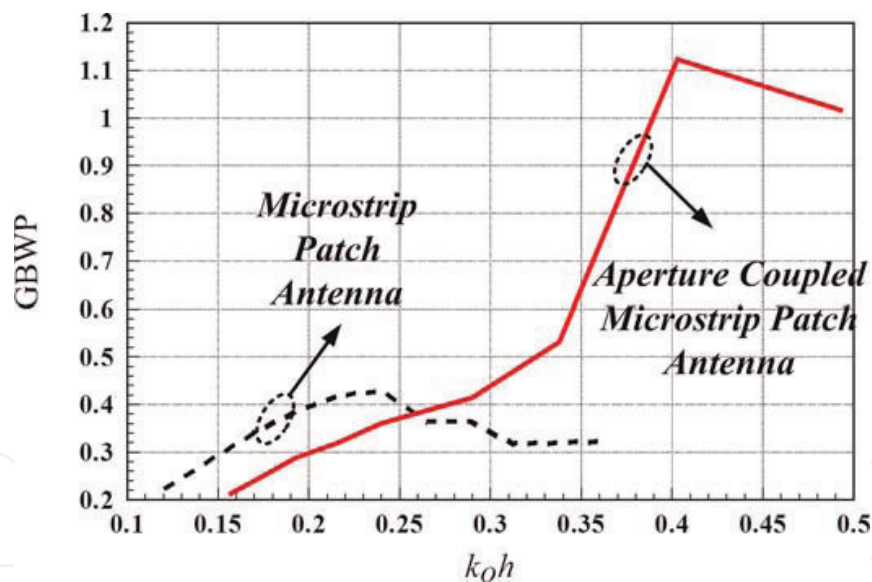**Figure 3.** GBWP vs. k_0h for different aspect ratios.

Figure 4. GBWP vs. k_0h comparison between aperture coupled (nonresonant slot) microstrip antenna and pin-feed microstrip antenna (antenna substrate is air and ε_r for feed substrate of aperture coupled antenna is 2.2).

3.2. Aperture coupled microstrip patch antenna

A typical aperture-coupled microstrip patch antenna is shown in **Figure 5**, with a slight difference. The structure shown below has a secondary patch named "the parasitic patch." This parasitic element is placed in order to give the structure a double resonant characteristic to enhance the bandwidth. The key analysis in this section is to decide what type of aperture structure is the optimum based on GBWP.
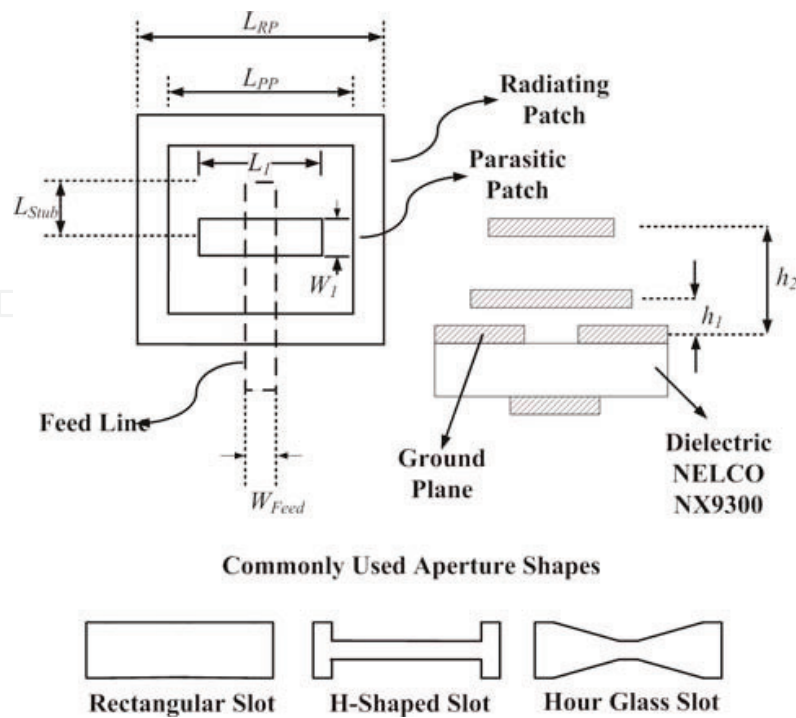
Figure 5. Aperture-coupled antenna and possible aperture shapes.

To compare the antenna performances, FOM_1 (figure-of-merit 1) is defined as GBWP (Eq. (11)) without considering the electrical height and half power beam width (HPBW) of the antenna. We also studied resonant slot coupled patch antenna, pin-feed microstrip antenna (MSA) and resonant slot with two stacked patches (three resonators), all optimized for performance. The results are shown in **Table 2**.

We observe that all nonresonant slot coupled antennas have very similar performance, but hourglass is slightly better than the others. A resonant slot with two stacked patches achieves almost 54% BW.

Antenna	Gain (dBi)	BW	k_0h	FOM_1
H-shaped slot	7.87–9.06	0.275	0.837	2.088
Hour glass slot	7.88–9.07	0.283	0.837	2.150
Rectangular slot	7.89–9.04	0.275	0.837	2.083
Resonant slot	3.51–9.19	0.350	0.736	2.142
Three resonators	5.14–8.88	0.539	0.431	1.314
Pin-fed MSA	9.2–9.3	0.047	0.277	0.401

Table 2. Comparative study based on FOM1.

3.3. Design of a Ku band antenna

Earlier sections have led us to a conclusion on the topology of the element antenna. The final results show that an aperture-coupled stacked patch antenna with an hour-glass shaped

nonresonant aperture would be the best solution for the element antenna. **Figure 6** shows the structure of the antenna to be designed.
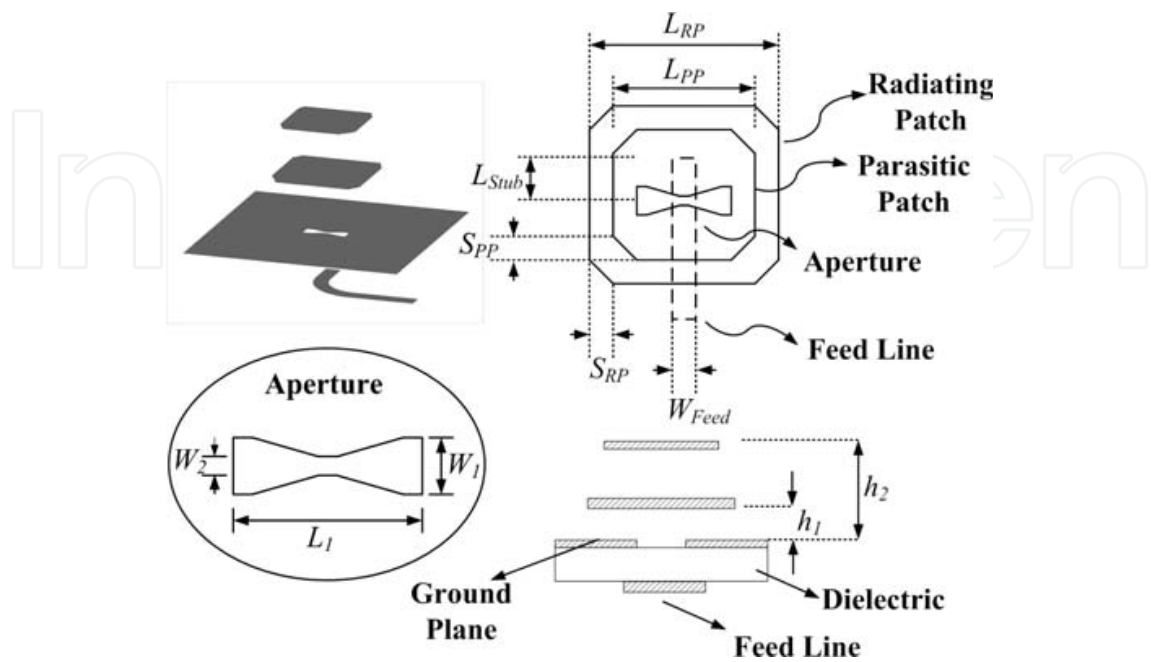

Figure 6. Aperture-coupled stacked microstrip patch antenna.
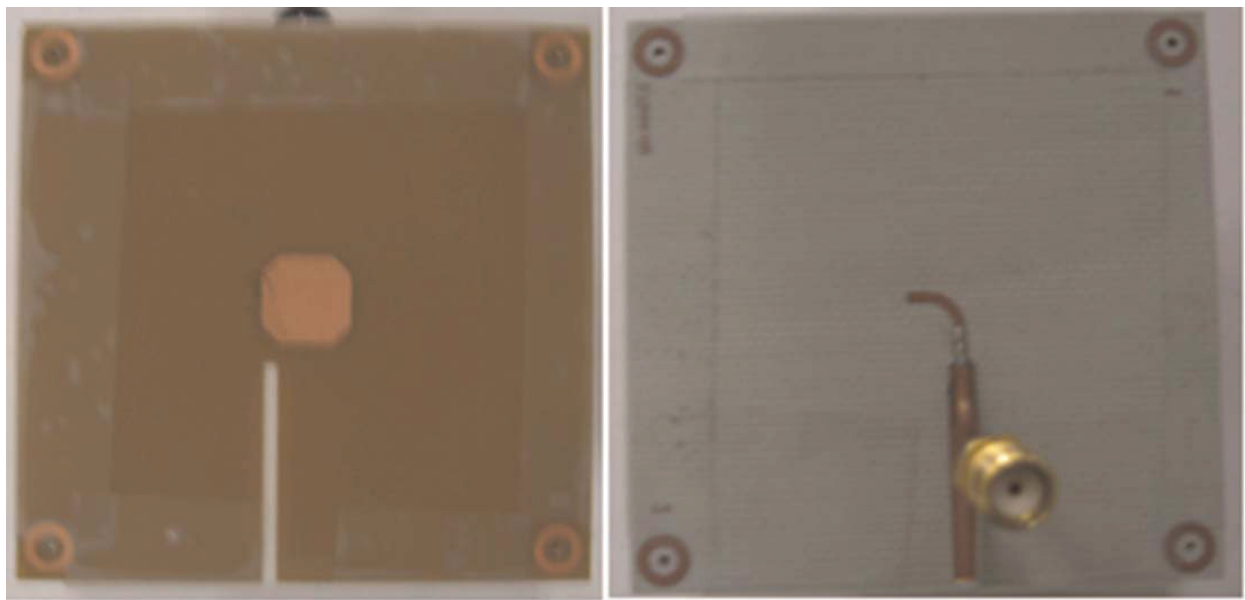

Figure 7. Antenna-prototype: top (patch) side and bottom (feedline) side.

The antenna was optimized through simulations in a commercial full-wave electromagnetic solver to give the best results possible, followed by this optimization the realized antenna is shown in **Figure 7**. Target band is the Ku band downlink frequencies. Radiating and parasitic

patches were formed on flexible PCBs with 75 μm thickness and were placed over the slots using Rohacell HF 31 foam (ε_r = 1.046, tanδ = 0.0017). Measurements were carried out in an anechoic chamber using R&S ZVA40 Network Analyzer, and measurement results are displayed in **Figure 8**. Impedance match bandwidth is defined as |S11| < -9.5 dB (VSWR < 2).

Simulations show that the antenna has 25% FBW with maximum broadside gain of 9.67 dBi at 11.24 GHz. Measured antenna has 29% FBW and maximum broadside gain of 9.5 dBi. In-band gain ripple is less than 0.5 dB, which is also desirable in phased array antenna applications. Broadside gain is greater than 9.3 dBi in 10.8–12.75 GHz frequency band. Vertical polarization principal plane (φ = 0°) radiation pattern at 11.9 GHz, center frequency of Ku band downlink, is shown in **Figure 9**. The HPBW is almost 80°. Due to its wide beamwidth, the antenna can be utilized in electronically beam-tilted phased array antennas. Measurements corroborate well with simulation results in terms of gain, impedance bandwidth, radiation patterns, and HPBW.
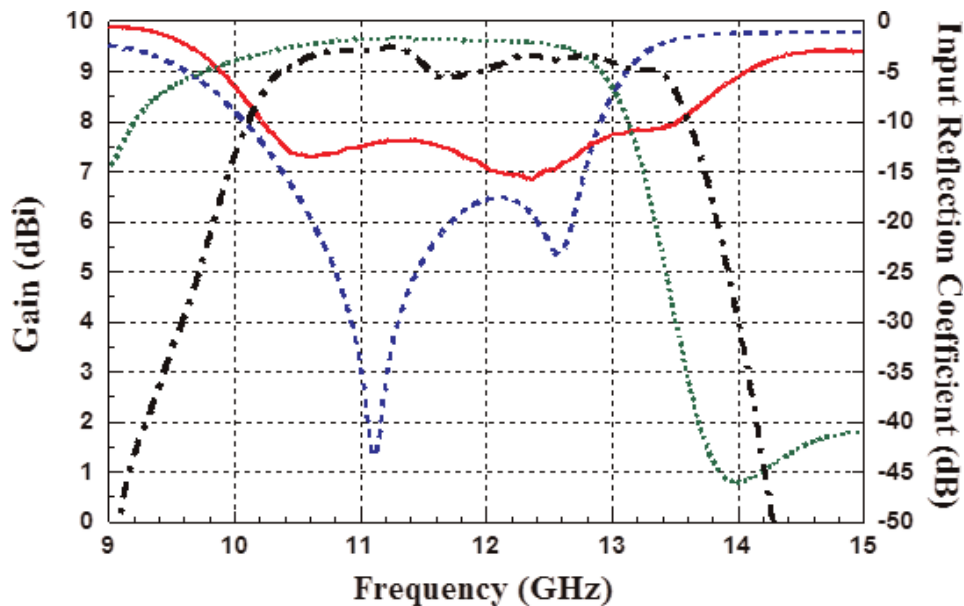

Figure 8. Simulated and measured, gain and input reflection coefficient vs. frequency graphs of aperture coupled antenna (▬▬▬ Measured Input Reflection Coefficient, ▬ · ▬ Measured Gain, •••••••• Simulated Gain, ▬ ▬ ▬ Simulated Input Reflection Coefficient).

3.4. Other FOM definitions and a comparative study with previous antenna designs

In a typical system design, minimum in-band gain is more critical than average gain to satisfy minimum target SNR. Hence, we modified FOM$_1$ in terms of minimum gain and electrical height of the antenna as:

$$\text{FOM}_2 = G_{\text{min}}\text{BW}\frac{1}{k_0 h} \tag{12}$$

where G_{min} represents the minimum gain throughout the band and $k_0 h$ represents electrical height ($2\pi h/\lambda$) at f_c. Finally, we define a third FOM to include HPBW as:
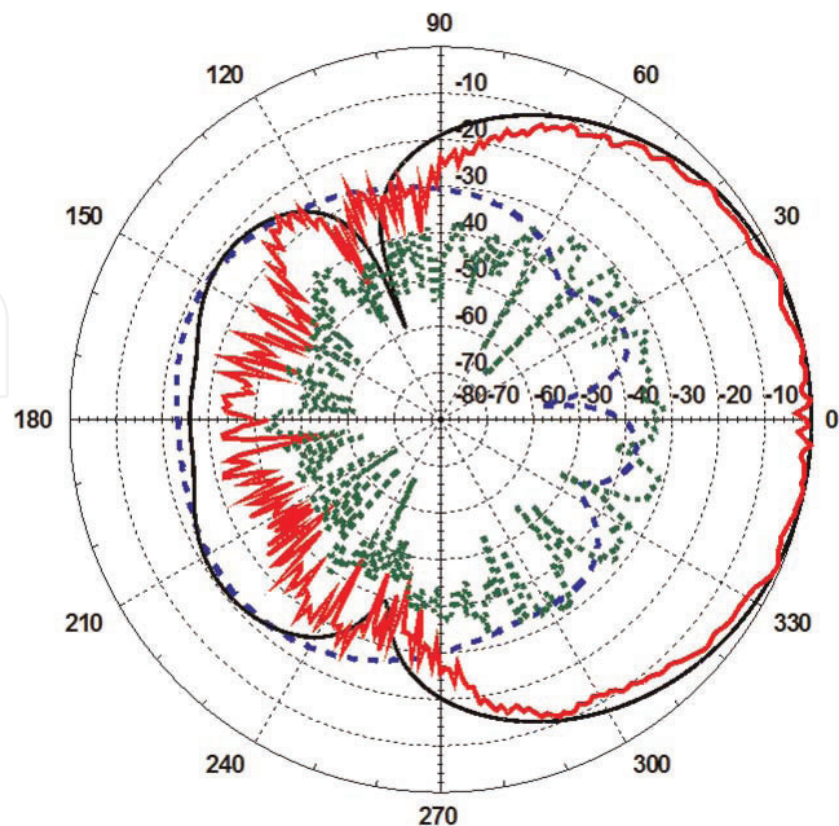
Figure 9. Simulated and measured, normalized gain patterns at 11.5 GHz (▬▬▬ Measured Co-Pol pattern, ▬▬▬ Simulated Co-Pol pattern, •••••••• Measured X-pol pattern, ▬ ▬ ▬ Simulated X-pol pattern).

$$\text{FOM}_3 = G_{\min}\left(\frac{\text{HPBW}}{\pi}\right)\text{BW}\frac{1}{k_0 h} \tag{13}$$

Table 3 shows a comparative study between this work and some of the previously designed antennas based on the three figure-of-merit definitions, bolded numbers show the best design

Antenna	Gain (dBi)	BW (%)	HPBW/π	$k_0 h$	FOM$_1$	FOM$_2$	FOM$_3$
This work	9–9.5	0.290	0.438	0.868	2.389	**2.118**	**0.929**
[12]	5–7	0.525	0.431	1.452	2.424	1.142	0.493
[14]	7–8.9	0.391	0.444	1.925	2.388	0.642	0.285
[15]	8.2–9.1	0.155	0.437	0.607	1.211	1.806	0.790
[21]	9–9.3	0.110	0.433	0.617	0.905	1.413	0.612
[21]	12–13.9	0.110	N/A	3.539	2.221	0.492	N/A
[22]	8–13.5	0.235	0.138	4.451	**3.485**	0.333	0.046
[23]	9.2–9.7	0.190	0.435	1.007	1.601	1.313	0.571
[24]	8.5–9.17	0.355	0.435	1.171	2.777	1.836	0.799
[25]	6.2 – 6.7	0.040	0.351	0.544	0.187	0.344	0.120

Table 3. Comparative study based on all three figure-of-merits.

based on defined FOM's. It is clear that values obtained in this work are very close to those from [14] in FOM_1 where electrical height is not taken into account. Also values obtained in [22] being the best solution, nearly all the other designs are better than this work. But when the physical dimensions, minimum gain, and half power beamwidths are taken into account; present work is better than all other antennas in FOM_2 and FOM_3. We believe FOM_2 and FOM_3 are critical in array applications as the height of the antenna can be further increased with suspended or inverted substrate etched structures to enhance gain at the expense of increased antenna profile.

4. Array and hybrid microstrip/waveguide feed network design

In third section and its sub-sections, the design of an aperture-coupled stacked microstrip patch antenna was accomplished and the antenna was compared with previous studies. It has proven its value accomplishing the figures-of-merit defined. This section will focus on the array synthesis and the feed network design.

4.1. Array synthesis

There are multiple methods and formations possible to develop an antenna array capable of satisfying the specifications given in **Table 1**. Yet the most important specifications were the maximum dimensions and weight, which were supplied according to the needs of the industry. The system diameter must not exceed 75 cm, the height must be less than 7 cm and the weight must be less than 5 kg. The antenna will have two panels, one for each polarization. Based on these facts, the array should cover an area with lengths less than 73cm × 20 cm. Using array theory, it is possible to synthesize an array of 256 elements with the area of given dimensions. **Figure 10** shows the layout of a two-dimensional array.
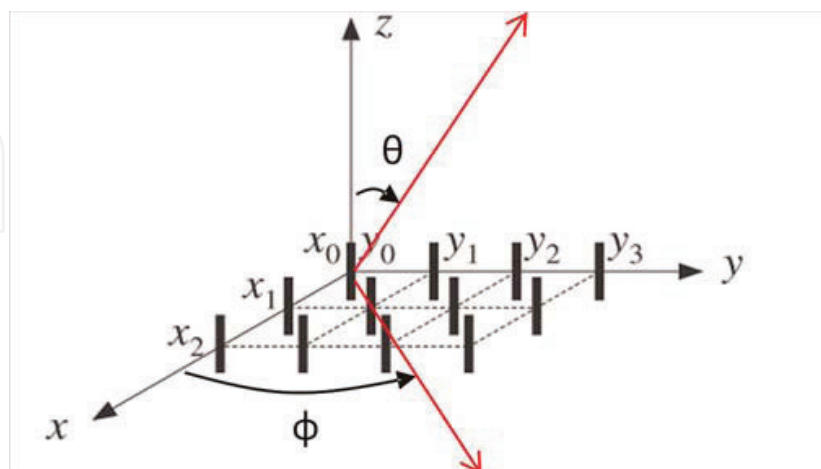

Figure 10. Two-dimensional array.

Let us say that, n and m are the number of elements in the x and y directions, respectively. The interelement spacing in the x and y directions are d_x and d_y respectively. $xs_{n,m}$ and $ys_{n,m}$ are the

positions of the source antennas on the (x,y) coordinate system. θ_0 and φ_0 are the angles pointing the main beam direction of the antenna pattern. The current distribution of each element being $I_{a,b}$, the array factor of such an array can be written as follows:

$$AF(\theta, \varphi) = \sum_{b=1}^{m} \sum_{a=1}^{n} I_{a,b} e^{j\{\beta[xs_{n,m}(\sin\theta\cos\varphi - \sin\theta_0\cos\varphi_0) + ys_{n,m}(\sin\theta\cos\varphi - \sin\theta_0\cos\varphi_0)]\}} \tag{14}$$

The array antenna in this application should have the highest gain possible. Since the array is a receive-only structure, side lobe levels are not of utmost importance. HPBW in both elevation and azimuth axes are very important for the design due to the physical limits given in the specifications. A trade-off between azimuthal HPBW and gain has been made. For maximum gain, elements in the azimuth axis have been placed 0.82λ (d_y) apart. On the other hand, elements in the elevation axis have been placed 0.73λ (d_x) apart. Spacing in the elevation axis was set in that magnitude so that the phasing of each row would have an electrical phase shift of 90° for a beam pointing at the desired beam angle ($\theta_0 = 20°$, $\varphi_0 = 0°$). The array factor given in Eq. (14) would become:

$$AF(\theta, \varphi) = \sum_{b=1}^{32} \sum_{a=1}^{8} A_{a,b} e^{j\{2\pi[0.82(b-16.5)\left(\sin\theta\cos\varphi - \sin(20)\right) + 0.73(a-4.5)(\sin\theta\cos\varphi)]\} + \vartheta_{a,b}} \tag{15}$$

where $A_{a,b}$ is the magnitude of current at each element (which is 1, for uniform excitation) and $\vartheta_{a,b}$ is the electrical phasing of each element (90° between each row, uniform in the azimuth axis). **Figure 11** shows the elevation pattern of the synthesized array of 256 which consists of 8 rows and 32 columns.

4.2. Hybrid microstrip and waveguide feed network

Ohmic and dielectric losses tremendously increase in high frequencies, therefore a dramatic loss is perceived by the feed network for large arrays. We must also put the surface wave excitation and radiation losses into account concerning the feed network. The reason that corporate microstrip feed network becomes immensely difficult when combining 256 elements is thus the electrically long microstrip lines. To overcome feed network loss, series feed, parallel feed, series-parallel feed, all waveguide feed and waveguide-microstrip hybrid feed, various techniques were proposed in the past. Waveguide-only feed, i.e., each antenna element being fed into the waveguide, is not attractive due to cost and weight of the die-cast structure. Series, parallel, and their combinations exhibit poor bandwidth performance and only work well for narrowband systems. Most suitable choice would be hybrid microstrip and waveguide feed system, but the size of the corporate feed for the subarray must be carefully determined. Dominant mode waveguides are known for their low loss properties. The crucial aspect of design of such a hybrid structure would be microstrip-to-waveguide transition. For this design, the waveguide must be 6 mm below the feedline, on the other side of a reflecting ground. In the following parts of this section; the design of a low loss microstrip-to-waveguide transition, a detailed analysis on microstrip line and waveguide losses will be discussed and finally the optimum solution for the feed network structure will be calculated.
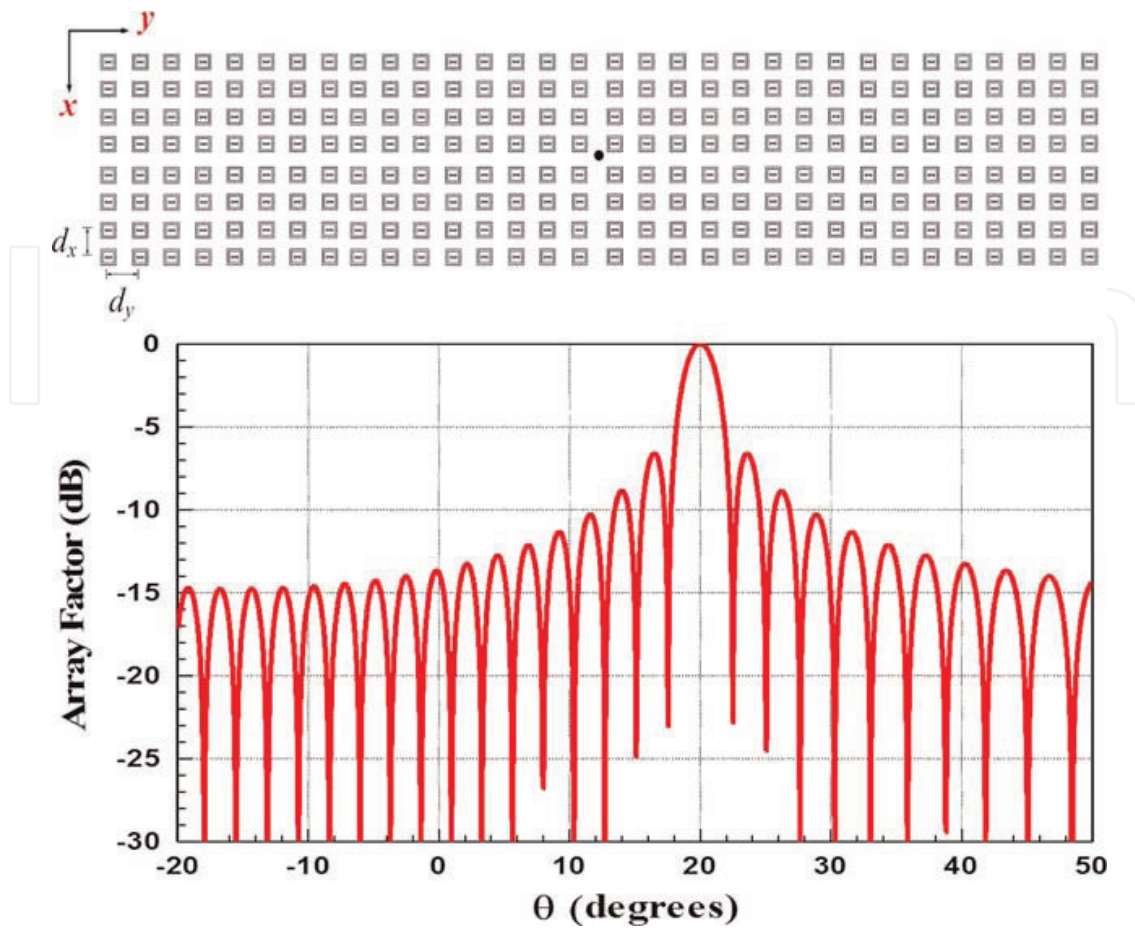
Figure 11. Array factor elevation pattern of synthesized array.

4.2.1. Microstrip feed network losses

The well-known reasons for loss in microstrip lines are conductor losses, dielectric losses, radiation losses, and surface wave losses. Regarding the fields within two guided-wave media, TEM waves do not propagate in microstrip lines. When the longitudinal components of the fields are significantly diminished compared to transverse components, the quasi-TEM approximation is applicable. Equations given below can be found in almost every book about antennas and microwave theory. Although the accuracy of these equations is not that liable for the Ku band, it will provide a fairly satisfying approximation for determining the dimensions of the subarray feed network. Dielectric properties of the substrate that will be used are; dielectric constant (ε_r) 3, loss tangent ($\tan\delta$) 0.0023, thickness (h) 0.5 mm, and copper thickness (t) 35 µm.

The frequency for which the effects of dispersion that can be neglected is calculated from (for h given in mm, f_{dis} is in GHz):

$$f_{dis} = 0.03\sqrt{\frac{Z_0}{h\sqrt{\varepsilon_r - 1}}} \tag{16}$$

f_{dis} is calculated to be nearly 8 GHz. For a Ku band application, the dispersion effects cannot be neglected. The effects of dispersion mostly affect the relative dielectric constant. Calculations can be modified to include these effects with varying frequencies.

Let W be the width of the feedline and t the copper thickness, the effective feedline width to dielectric thickness ratio can be calculated as:

$$\frac{W_{\text{eff}}}{h} = \frac{W}{h} + \frac{t}{\pi h}\left(1 + \ln\frac{2h}{t}\right) \quad for \; {}^W\!/_h \geq{}^1\!/_2 \; \pi \tag{17}$$

$$\frac{W_{\text{eff}}}{h} = \frac{W}{h} + \frac{t}{\pi h}\left(1 + \ln\frac{4\pi W}{t}\right) \quad for \; {}^W\!/_h \leq{}^1\!/_2 \; \pi \tag{18}$$

Effective dielectric constant can be calculated as:

$$\varepsilon_{\text{eff}} = \frac{\varepsilon_r + 1}{2} + \frac{\varepsilon_r - 1}{2}\left(1 + 12\frac{h}{W_{\text{eff}}}\right)^{-1/2} \quad for \; {}^{W_{\text{eff}}}\!/_h \geq 1 \tag{19}$$

$$\varepsilon_{\text{eff}} = \frac{\varepsilon_r + 1}{2} + \frac{\varepsilon_r - 1}{2}\left[\left(1 + 12\frac{h}{W_{\text{eff}}}\right)^{-1/2} + 0.04\left(1 - \frac{W_{\text{eff}}}{h}\right)^2\right] \quad for \; {}^{W_{\text{eff}}}\!/_h \leq 1 \tag{20}$$

Effects of frequency variations on ε_{eff}:

$$\varepsilon_{\text{eff}}(f) = \frac{\varepsilon_r - \varepsilon_{\text{eff}}}{1 + (0.6 + 0.009 Z_0)\left(\frac{8 f \pi h}{Z_0}\right)^2} \tag{21}$$

Characteristic impedance Z_0 can be calculated by:

$$Z_0 = \frac{60}{\sqrt{\varepsilon_{\text{eff}}(f)}} \ln\left(8\frac{h}{W_{\text{eff}}} + 0.25\frac{W_{\text{eff}}}{h}\right) \quad for \; {}^{W_{\text{eff}}}\!/_h \geq 1 \tag{22}$$

$$Z_0 = \frac{{}^{120\pi}\!/_{\sqrt{\varepsilon_{\text{eff}}(f)}}}{\frac{W_{\text{eff}}}{h} + 1.393 + 0.667\ln\left(\frac{W_{\text{eff}}}{h} + 1.44\right)} \quad for \; {}^{W_{\text{eff}}}\!/_h \leq 1 \tag{23}$$

Wavelength:

$$\lambda = \frac{\lambda_0}{\sqrt{\varepsilon_{\text{eff}}(f)}}\left[\frac{\varepsilon_{\text{eff}}(f)}{1 + 0.63\left(\varepsilon_{\text{eff}}(f) - 1\right)\left(\frac{W_{\text{eff}}}{h}\right)^{0.1255}}\right]^{1/2} \quad for \; {}^{W_{\text{eff}}}\!/_h \geq 0.6 \tag{24}$$

$$\lambda = \frac{\lambda_0}{\sqrt{\varepsilon_{\text{eff}}(f)}}\left[\frac{\varepsilon_{\text{eff}}(f)}{1 + 0.6\left(\varepsilon_{\text{eff}}(f) - 1\right)\left(\frac{W_{\text{eff}}}{h}\right)^{0.0297}}\right]^{1/2} \quad for \; {}^{W_{\text{eff}}}\!/_h \leq 0.6 \tag{25}$$

From these equations, one can easily calculate the width (W) for 50 Ω line at the Ku band mid frequency, to be 1.055 mm. The total loss in a feedline can be calculated from the sum of the attenuation constants for α_c (conductor loss), α_d (dielectric loss), α_{surf} (surface loss) and α_{rad} (radiation loss). Since we are trying to practically calculate the losses of a microstrip feed network for an antenna array, the length of the feedline will be found to be greater than 5λ.

For this reason, the effects of radiation and surface wave losses can be neglected since their effects are small compared to the conductor and dielectric losses.

Conductor losses can be calculated by:

$$\alpha_c = 20 \log e^{\frac{1}{Z_0 W_{\text{eff}}} \sqrt{\frac{\pi f \mu_0}{\sigma_c}}} \tag{26}$$

Dielectric losses can be calculated by:

$$\alpha_d = 20 \log e^{\frac{2\pi \varepsilon_r \left(\frac{\varepsilon_{\text{eff}}(f) - 1}{\varepsilon_r - 1} \right) \tan \delta}{\lambda(\varepsilon_r - 1)\sqrt{\varepsilon_{\text{eff}}(f)}}} \tag{27}$$

4.2.2. Microstrip to waveguide transition losses

The transition geometry involves copper disk and dielectric loaded pin for wideband match and low loss. The geometry of the transition is illustrated in **Figure 12**. In order to register all ohmic losses of this design, the transition was modeled using a full-wave electromagnetics solver where waveguide is aluminum and the probe is copper. Simulated results for insertion loss and transmission loss are shown in **Figure 12**. Prototype of the disk-loaded transition was manufactured and measurements were carried out. Input reflection coefficient was below 15 dB and the loss for this transition was measured to be 0.78 ± 0.02 dB in the desired frequency band.

4.2.3. Waveguide combiner losses

In hybrid system, one must take the loss in the waveguide combiner into account as well for quantification. Instead of a typical E-type combiner, an H-type waveguide was chosen. The major reason to prefer this design was to decrease the height of the WR75 waveguide. Because the electric field lines are set parallel to longitudinal axis of the guide. Unlike the E-plane combiner, the output ports are in phase with each other as well resulting in no need for phase compensation. Moreover, it is easier to realize this waveguide since one is able to cut into one of the longer sections of waveguide in order to machine its remaining part from die-cast as well. Summary of all losses are presented in **Table 4**. Given these parameters, the size and form of the subarrays and waveguide sections can be designed.

4.2.4. Optimizing the hybrid feed network

An optimization problem for minimum feed network loss can be formulated and solved for subarray size. Layout of a general array is illustrated in **Figure 13**. Number of elements in x- and y-directions is denoted as N and M, respectively. Let N_S and M_S represent the number of elements in the subarray.

The number of levels for single output can be expressed as:

$$\log_2 NM = \log_2 N_s M_s + \left(\log_2 \frac{N}{N_s} + \log_2 \frac{M}{M_s} \right) \tag{28}$$

where $\log_2 N_S M_S$ and $(\log_2 N/N_S + \log_2 M/M_S)$ represent number of levels in the subarray and in the waveguide, respectively. Loss in the hybrid combiner can be stated as:
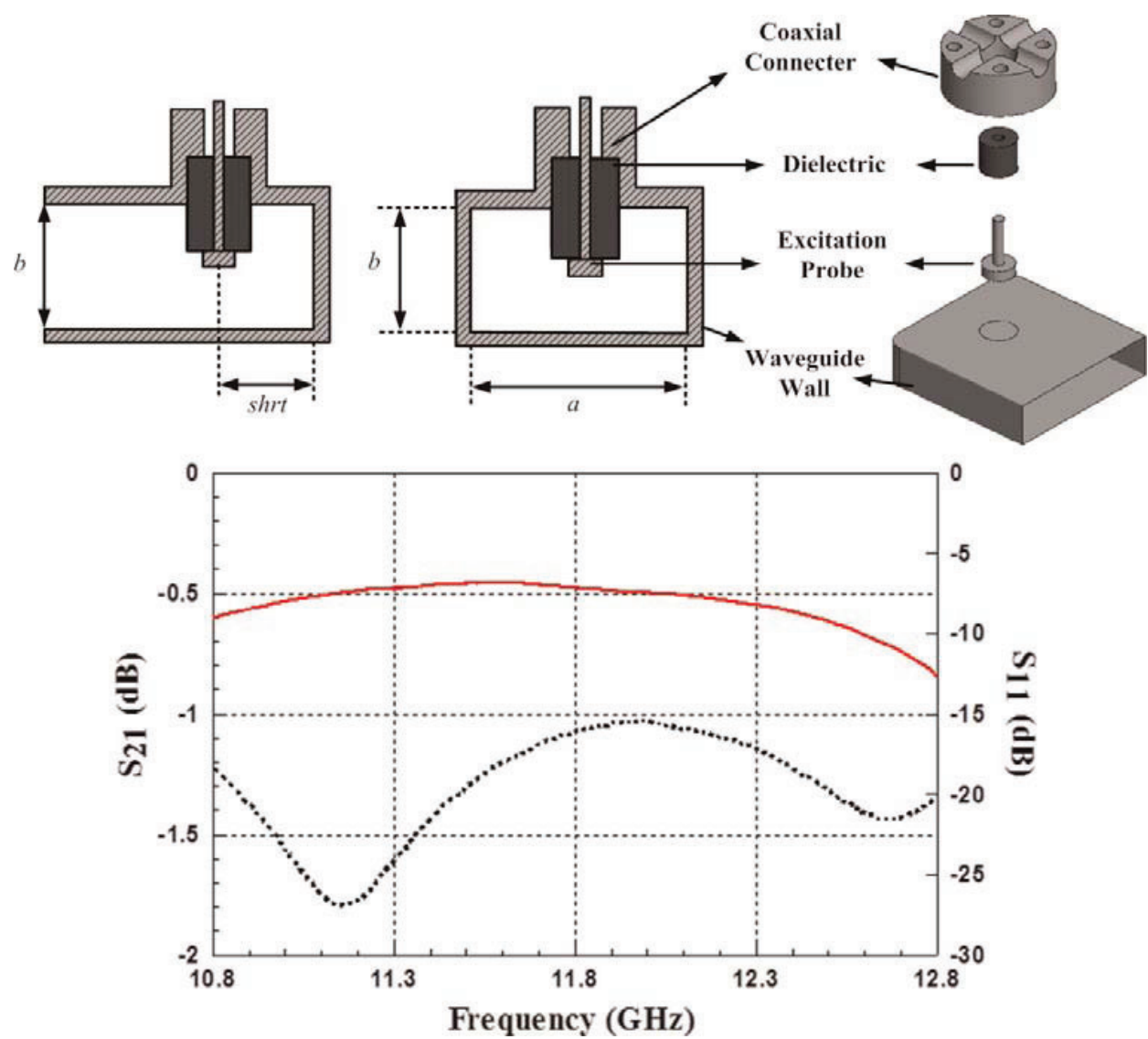
Figure 12. Microstrip line to waveguide transition and simulation results.

$$\left(\log_2 \frac{N}{N_s} + \log_2 \frac{M}{M_s}\right)L_{T,WG} + L_{TRANS} = L_1 \tag{29}$$

where $L_{T,WG}$ and L_{TRANS} are waveguide T-junction losses and microstrip to waveguide transition losses. A single transition is found to be effective while calculating the corporate feed

Component	Value
Microstrip line	0.072 dB/cm
Microstrip T-junction	0.11 dB
Microstrip-to-waveguide transition	0.78 dB
Waveguide T-junction	0.12 dB

Table 4. Summary of losses.
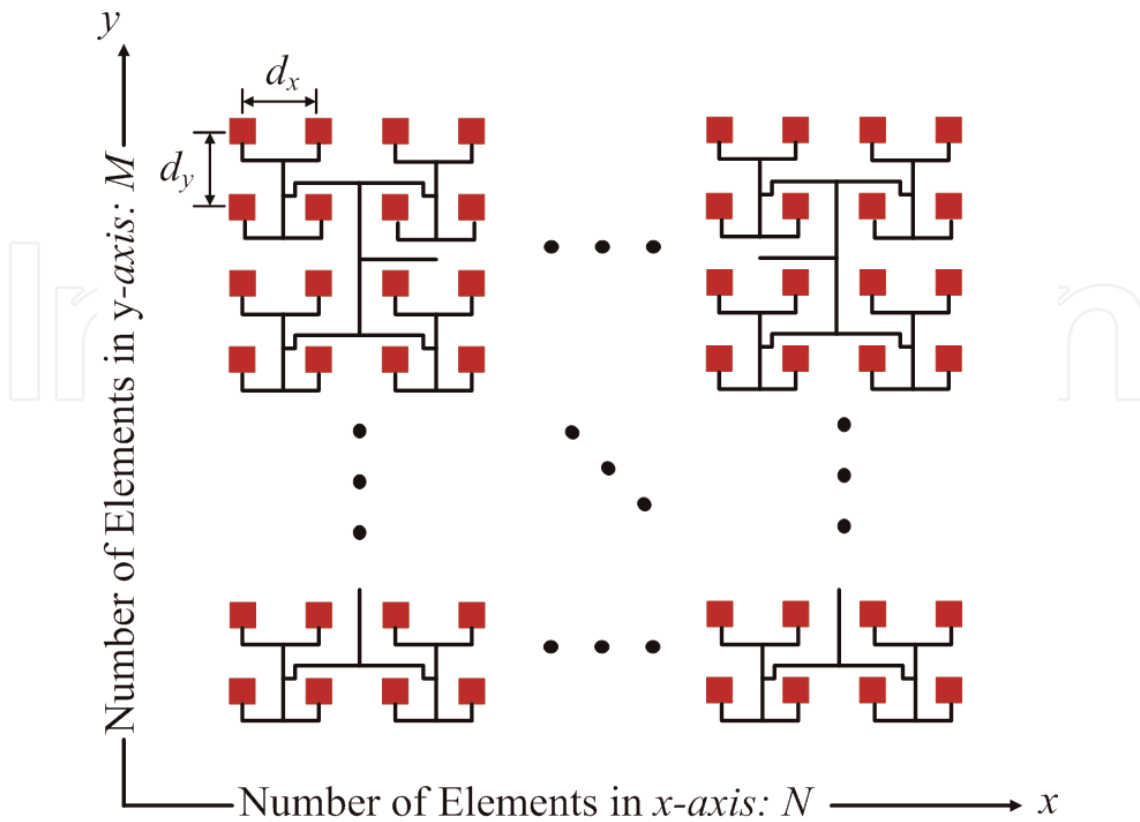
Figure 13. Layout of the feed network.

network loss in spite of the various (NM/N_SM_S) transitions in the waveguide. Loss in microstrip lines could be written as follows:

$$\left(\frac{d_x + d_y}{2} + \left(\frac{N_s}{2}-1\right)d_x + \left(\frac{M_s}{2}-1\right)d_y\right)L_{MS} + (\log_2 N_s + \log_2 M_s)L_{T,MS} = L_2 \qquad (30)$$

where d_x, d_y represent interelement spacing in x and y directions, and denote microstrip T-junction loss and microstrip line loss, respectively. Microstrip line loss includes ohmic and dielectric losses and it is calculated for a 50 Ω straight line section. Then, total loss becomes:

$$L_{tot} = L_1 + L_2 \qquad (31)$$

Furthermore, for corporate feed N, M, N_S and M_S must be multiples of 2, i.e., $N = 2^n$, $M = 2^m$, $N_s = 2^{n_s}$, and $M_s = 2^{m_s}$. Total loss can be restated as:

$$(n-n_s + m-m_s)L_{T,WG} + (n_s + m_s)L_{T,MS} + L_{TRANS} + (2^{n_s-1}d_x + 2^{m_s-1}d_y + l)L_{MS} = L_{tot} \qquad (32)$$

where l represents $-(d_x+d_y)/2$. Optimization function for minimization of loss for subarray size n_s and m_s can be formulated as follows:

$$minimize\ L_{tot}(n_s, m_s) \forall \quad n_s, m_s \in Z^+$$
$$Subject\ to$$
$$1 \leq n_s \leq \min(n, m) \tag{33}$$
$$1 \leq m_s \leq \min(n, m)$$
$$w(n_s, m_s) \leq 3\text{kg}$$

where $w(n_s, m_s)$ is the weight of the waveguide combiner, and dimensions of the subarray cannot is determined to be smaller than the full array size in all directions. The waveguide feed network consists most of the weight. Differing structures in the range of 4:1 to 64:1 gave way to the design of different waveguide feed networks (commercial full-wave electromagnetic solver) and models (CAD program for mechanical design). The weights of waveguide combiners were calculated according to aluminum alloy 6068 used in die-cast machines. Consequently, it was found that the required weight condition could only be reached for equal to 8:1 or smaller combiner structures. For instance, a 16:1 waveguide combiner (in which the elements in the subarray are 16) weighs 4.3 kg. Hence, the constraint on weight is replaced with $(n_s + m_s) > 5$. At a minimum of 32 elements is required in x-direction to obtain 3° HPBW in azimuth because a sum of 256 elements ($n + m = 8$) is utilized in the full array. Hence, m and n are set to 3 and 5, respectively (8 and 32 elements). It is now possible to have a solution for the optimization issue for subarray dimensions (n_s, m_s). Constrained nonlinear optimization was utilized to find (n_s, m_s) as (3, 2), and the optimal solution was found to have total loss of 2.16 dB. Since waveguide and microstrip T-junctions were overestimated, the realized loss will probably be lower than the calculated value.

The size of the subarray is set to 4 × 8 (32 elements total) and the subarrays are combined as 8:1 in the waveguide. We also observed that if we were able to use an alternative material such as electro-form-plated dielectric material, it was possible to reduce weight, which would enable a larger combiner that had less total loss.

5. Realization of the Ku band antenna and measurement results

The previous sections have led to the conclusion that the 256-element array antenna would consist of 8 rows and 32 columns. Further analysis on losses in the feed network components has shown that four row, eight column (32 elements) subarrays, where antenna elements are combined by microstrip feedline networks would give optimal performance and have an acceptable loss. Eight subarrays will then be combined by a reduced height waveguide combiner. This section will conclude with the design of each component and build both the vertical and horizontal polarization arrays.

5.1. Design of 4 × 8 (32-element) arrays

The Ku band array antenna is divided into eight subarrays for each polarization. Within each subarray, corporate feed network is used. Although corporate feed network has more loss than parallel feed network, it has much wider impedance bandwidth when tapered microstrip lines and tapered T-junctions are used. Each antenna input was defined as a 50

Ω port and *S*-parameters of 33-port network (32 for antennas and 1 for output port) were optimized for match, uniform power distribution, bandwidth, and minimum port-to-port coupling. Following that, as terminating loads in the feed network, simulated input impedance values of 32 antenna elements were placed. Finally, the layout was driven for the best match at the combined output. Vertical and horizontal subarrays for a fixed 20° elevation tilt are shown in **Figure 14**. Antiphase feeding between upper and lower parts of the vertical polarization subarray is used to reduce microstrip line lengths for required phasing (90°) between the rows of the array. The same technique was not possible to implement in the horizontal polarization subarray due to perpendicular orientation of coupling slots underneath feedlines. Element spacing along longer axis (azimuth tilt direction) and along shorter axis (elevation tilt direction) of the subarray is 0.82λ and 0.73λ, respectively.

Figures 15–17 show the realized antennas and their measurement results. The results show that the realized antennas have a minimum of 19 dBi gain throughout the desired bandwidth. A good matching lower than -10 dB is also achieved throughout the desired bandwidth.

5.2. Design of 8-to-1 waveguide power combiner

The optimum value for the waveguide combiner was calculated to be an 8-to-1 combiner, with reduced height. **Figure 18** shows a sketch drawing of the waveguide combiner.

Most of the losses and the power division take place in the bends and T-junctions. **Figure 19** shows a closer view of the waveguide junctions and bends. The parameters in **Figure 19** are the main optimization parameters. Optimizer goals were to minimize losses and have better impedance match less than -15 dB throughout the desired bandwidth. The most crucial component in the design of such divider is the position of the shorting probe. **Figure 20** shows the surface current of optimized combiner section. Optimized results are given in **Figure 21**. **Figure 21** (bottom graphic) shows the transition characteristic at all ports; simulations estimate the worst case, a loss of 0.5 dB.

5.3. Complete array realization and measurement results

The prototype antenna with all subarrays is built and the prototype is displayed in **Figure 22**. The performance of a dish antenna was taken as a reference for comparison. A parabolic reflector with corrugated circular feed horn (an existing commercial antenna) was also modeled for this purpose to be named "the reference antenna." This reference antenna exhibits similar performance to that of a 40 cm diameter dish antenna except that it has a lower profile. The simulation model with a great number of unknowns made it impossible to simulate full array with waveguide feed network. This resulted in the separate simulations of the planner array and the waveguide feed network to calculate both their S-parameters which led to the combination of these two results to get the final array performance. Measurements and simulations of planar array for input impedance match and gain at 20° tilt are displayed in **Figures 23** and **24**. Both the planar array and reference antenna showed in their gain simulations that they quantify similarly. Whereas
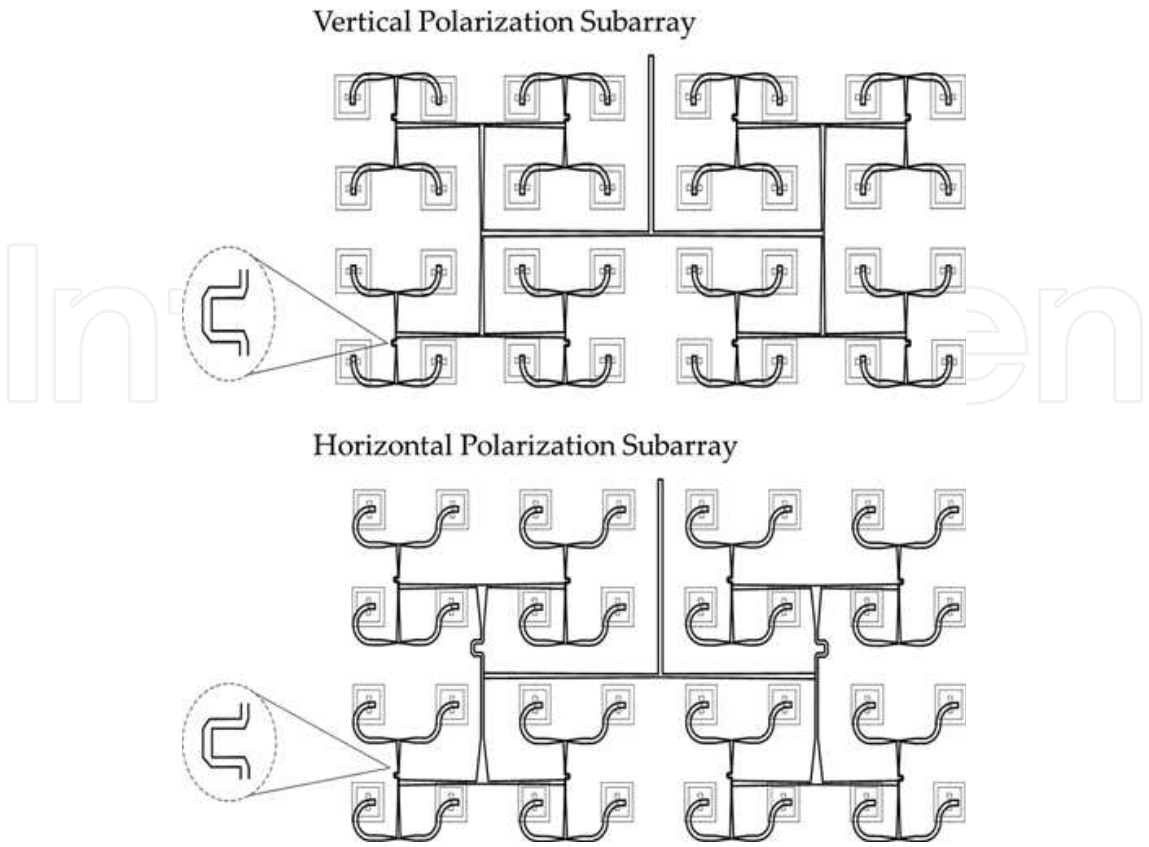
Vertical Polarization Subarray

Horizontal Polarization Subarray

Figure 14. 32 element subarray configurations for vertical polarization and horizontal polarization.
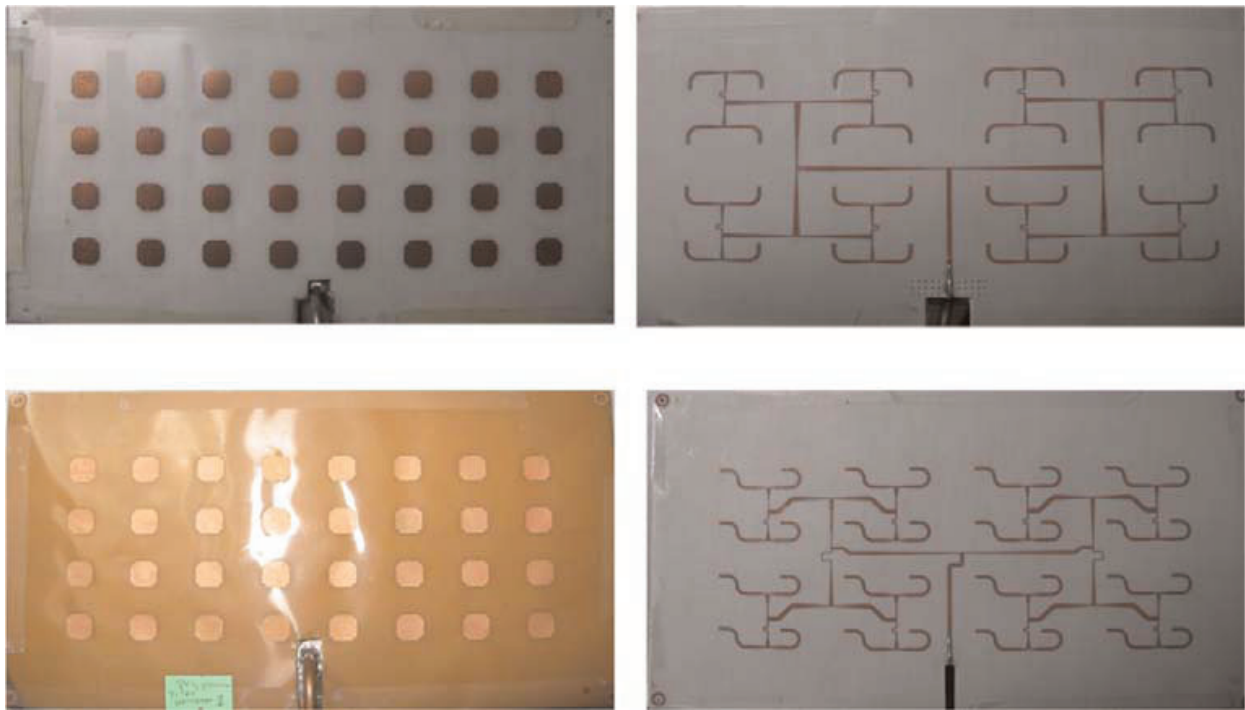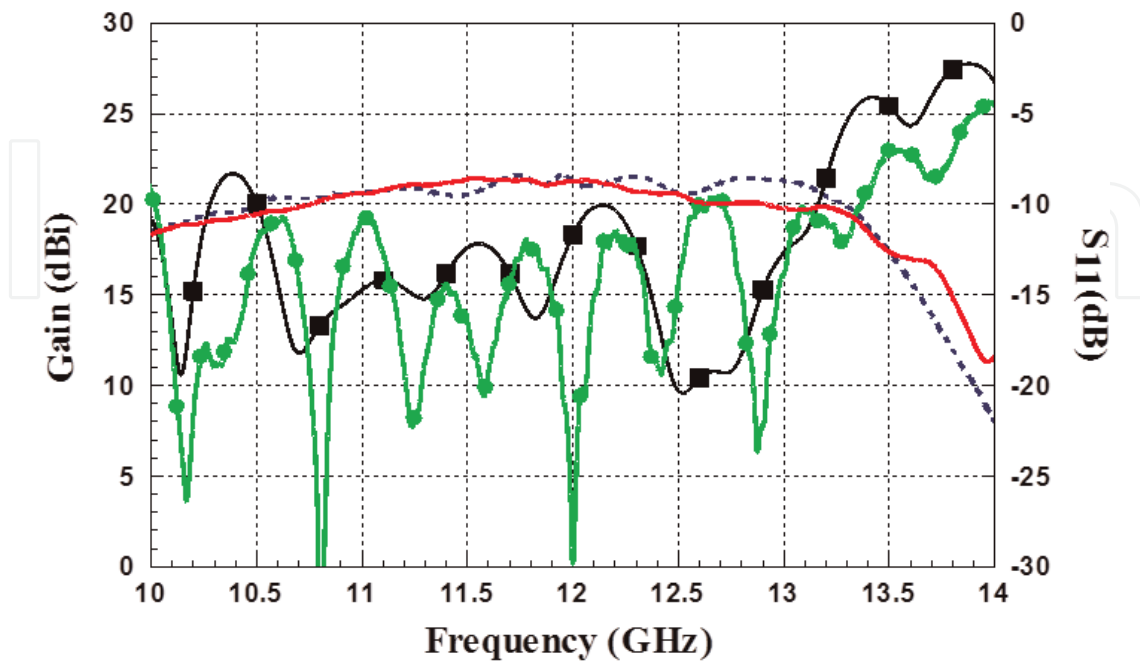
Figure 15. Realized vertical (top two pictures) and horizontal (bottom two pictures) subarray antennas.

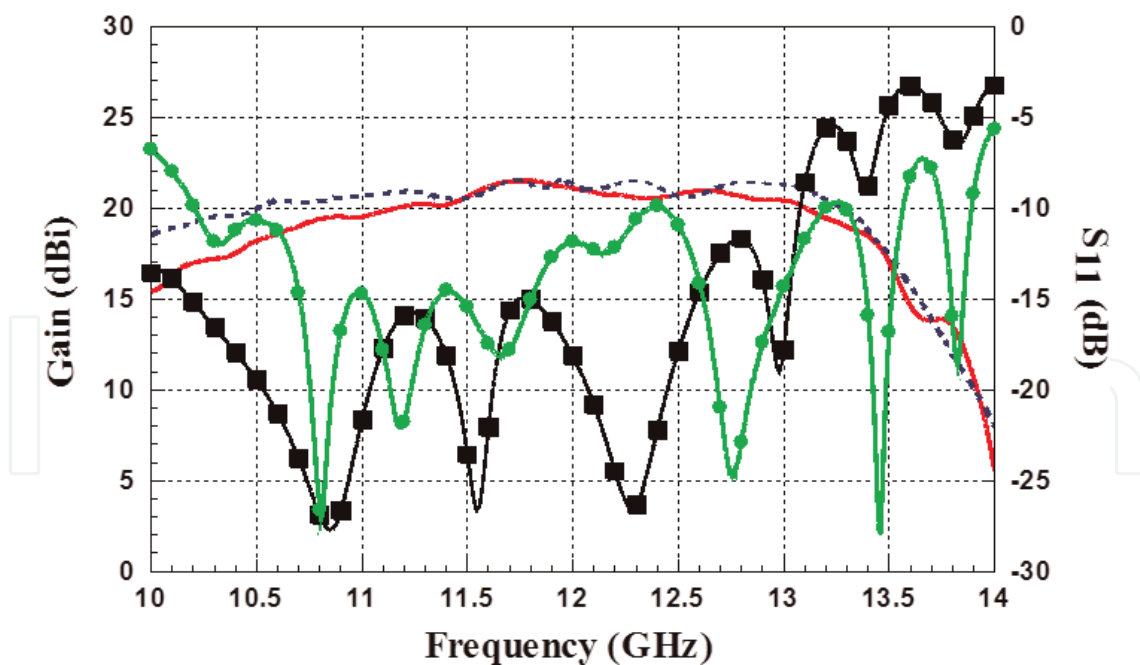## Vertical Polarization Subarray

Horizontal Polarization Subarray

Figure 16. Input reflection coefficient and gain of 32 element subarrays (▬▬▬ Measured Gain, ▬ ▬ Simulated Gain, ◆◆◆◆◆Measured S11, ■■■■■ Simulated S11).

when comes to measured gain, it was lower than the simulated gain because of the waveguide-to-coax adapter that was utilized in the measurements and for the nonideal

Vertical Polarization Subarray

Horizontal Polarization Subarray
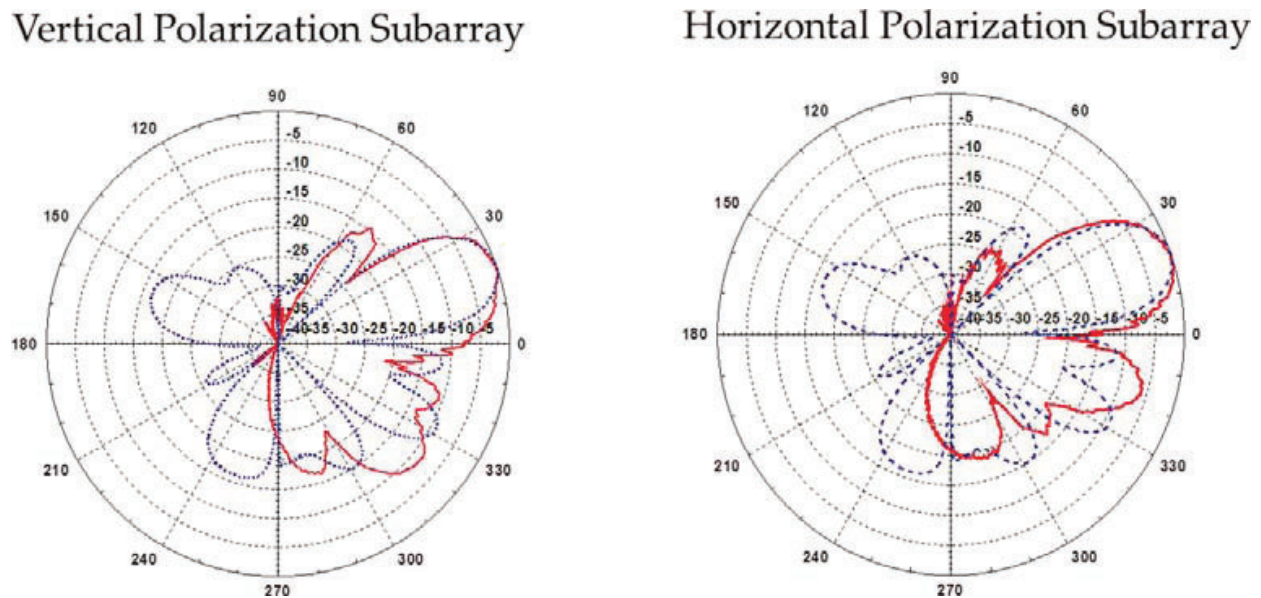
Figure 17. Normalized radiation pattern of 32-element subarray at 11.9 GHz (φ = 0°, elevation patterns) (▬▬▬ Measured Gain, ▬ ▬ Simulated Gain).
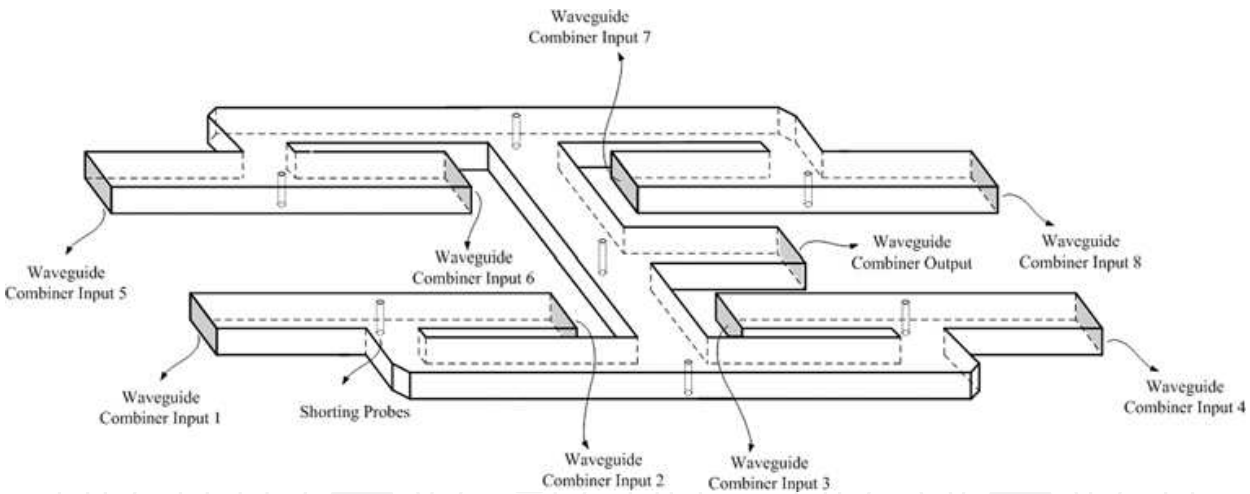
Figure 18. 8-to-1 power combiner.

simulation set-up. However, over entire target frequency band, the measured gain at desired tilt angle was found to be greater than 28.4 dBi. Planar array gain is 1.2 dB lower than the expected value from array theory. The radiation patterns of planar array at 20° tilt angle for azimuth and zenith cuts are shown in **Figure 25** and **Figure 26**. Measured HPBW$_\theta$ and HPBW$_\varphi$ are 8 and 2.5°, respectively. If the antenna was designed for broadside reception, its gain would have been definitely higher. The aperture efficiency of the planar array is between 57 and 67% over the target frequency band (**Figures 25–27**).
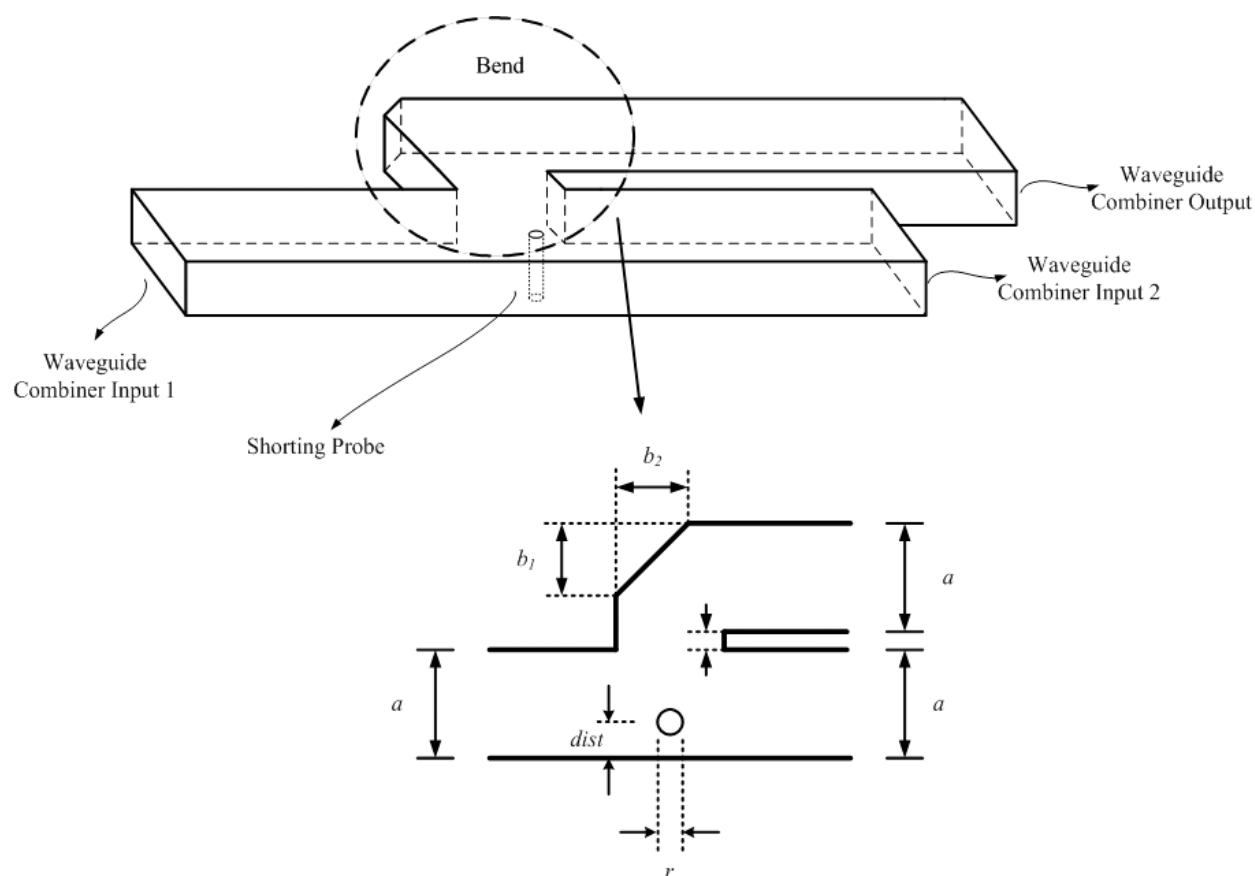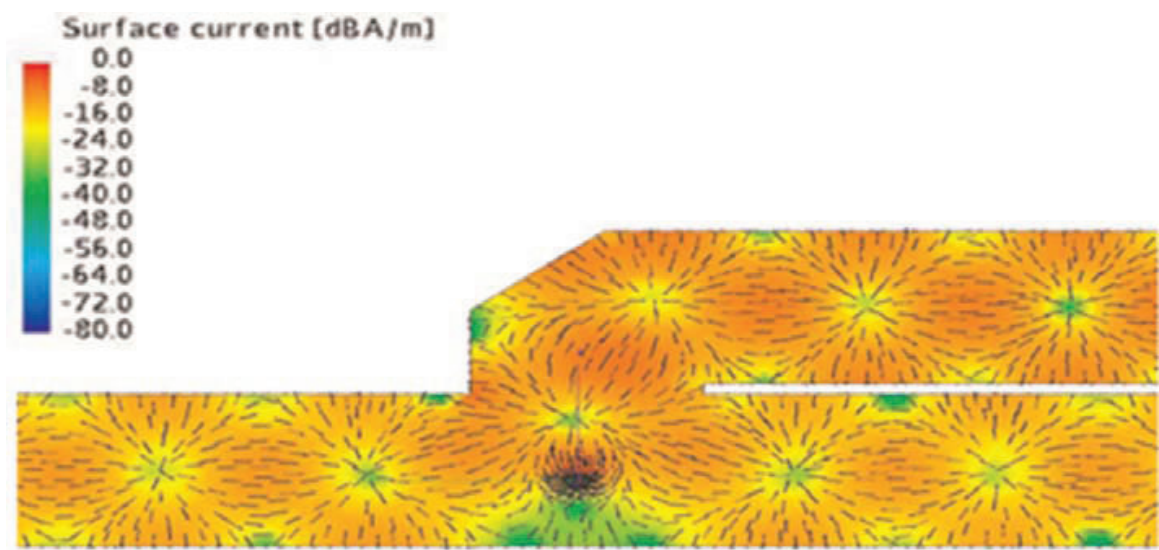
Figure 19. Waveguide bends and junctions.

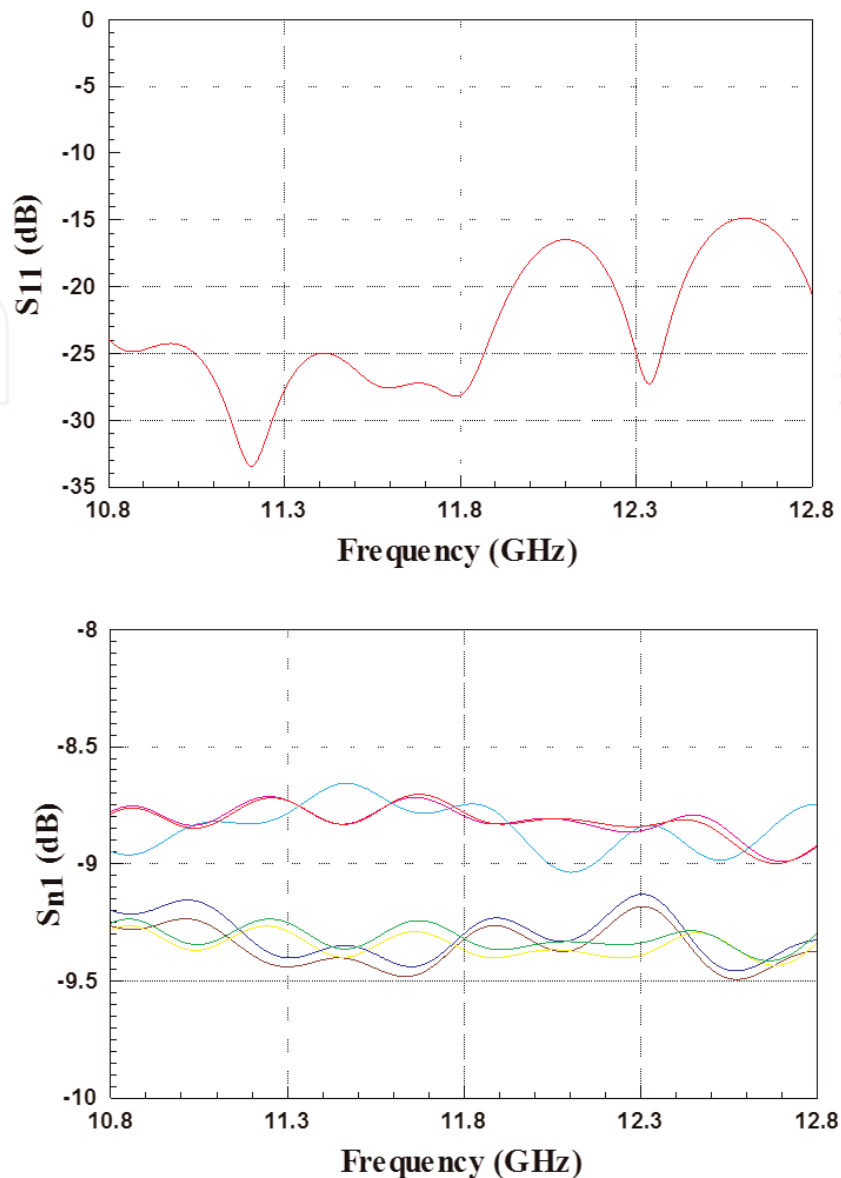**Figure 20.** Simulation of surface currents on the waveguide combiner.

Figure 21. Simulated input reflection coefficient at combiner output (top), simulated transmission coefficients of 8-to-1 power combiner (bottom).

The designed array antenna has also been field-tested for signal quality and satellite reception with an LNB and a receiver. The IF loop output of the receiver was connected to the Rohde & Schwarz FSH-8 GHz spectrum analyzer. Signal from transponders was observed to have an average CNR of 9.5 dB. In **Figure 28**, the measurement results are given. Reception quality retrieved from the receiver digital outputs was above 65%, which is slightly lower than that of the reference antenna (71%).
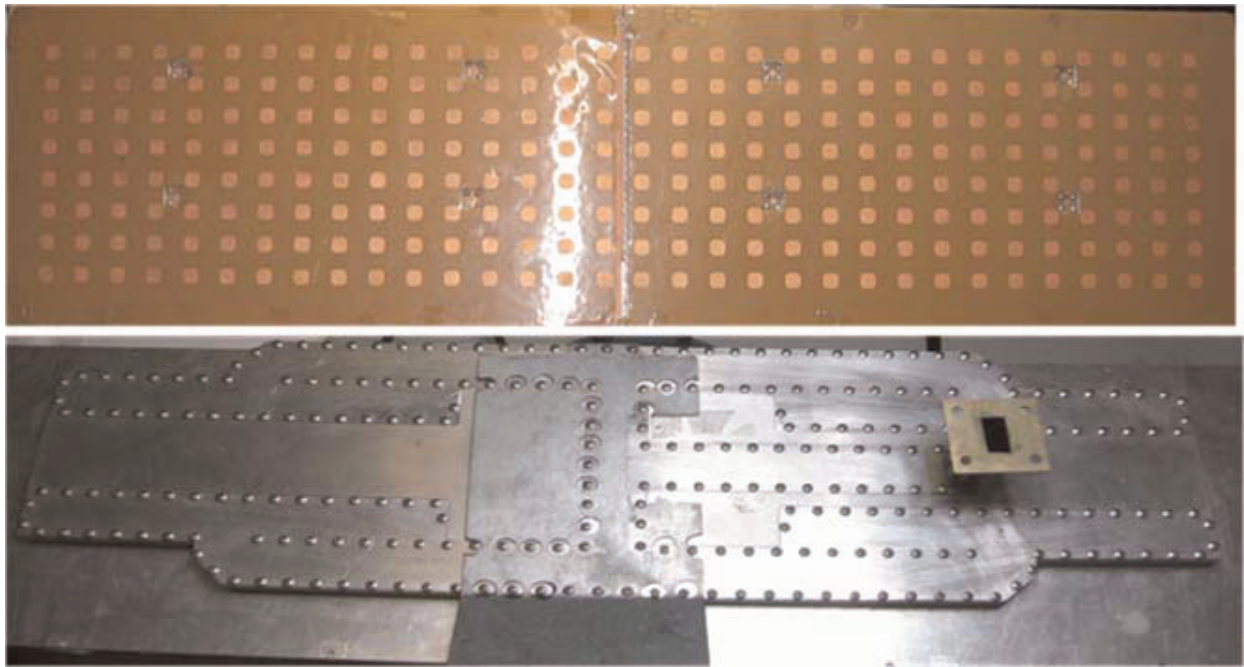
Figure 22. Prototype of vertical polarization 256-element array (dimensions: 70.73 cm × 18.23 cm × 2.43 cm, the height of the waveguide adapter is excluded from dimension).
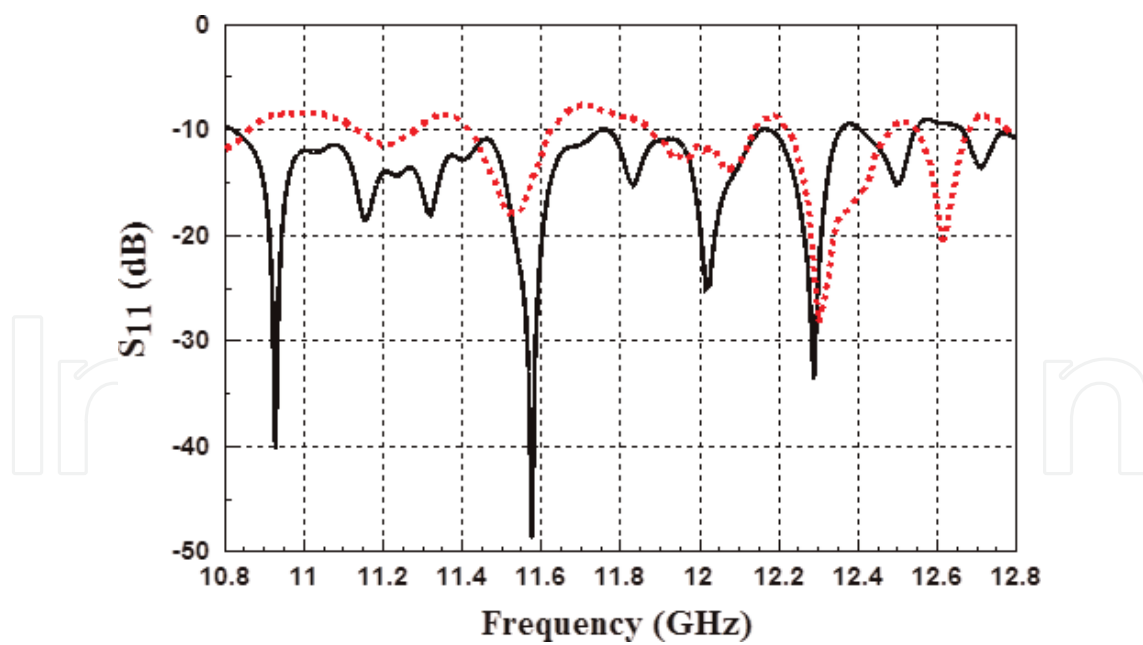

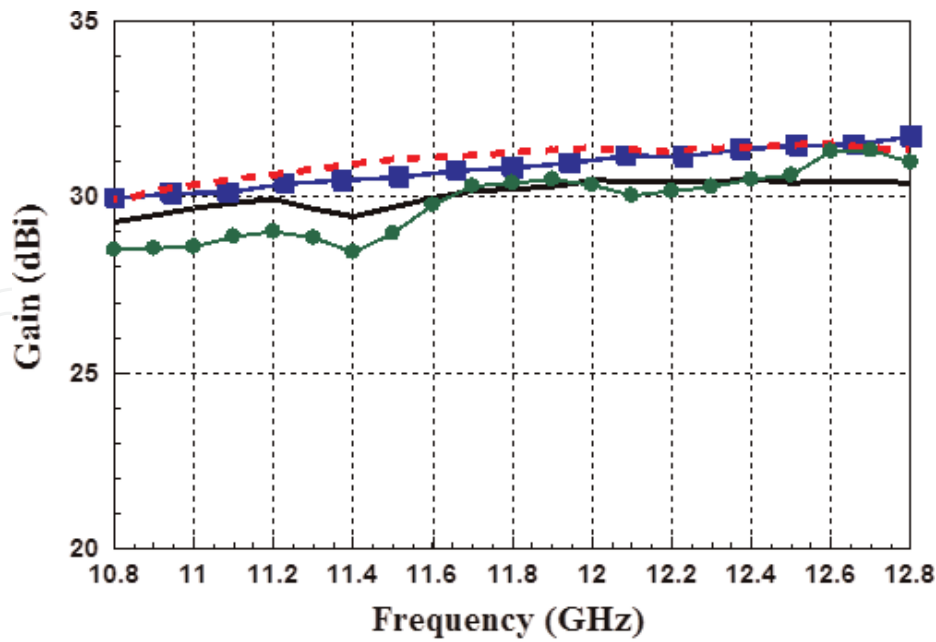**Figure 23.** S11 of array antenna. (▬▬▬ Measured, ▬ ▬ Simulated).

Figure 24. Gain of array antenna (θ = 20°cut) (▬▬▬ Measured Vertical Polarization, ●●●● Measured Horizontal Polarization, ▬ ▬ Simulated 256 Element Array, ▬■■■▬ Simulated Reference).
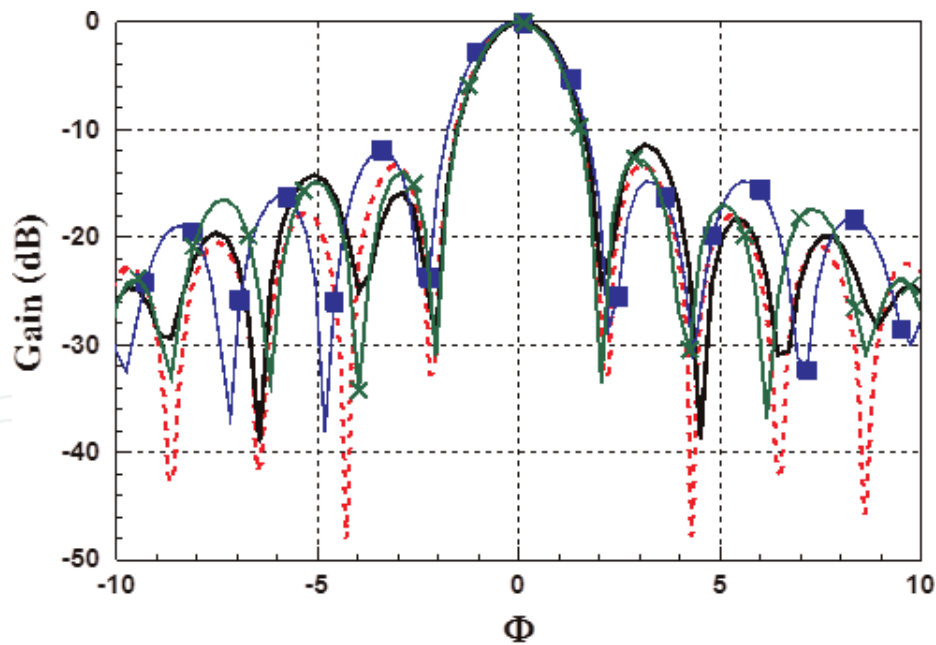

Figure 25. Radiation pattern of vertical polarized full array in azimuth plane (θ = 20°cut). (▬▬▬ Measured @ 11.9 GHz, ▬ ▬ Simulated @ 11.9 GHz, ▬■■■▬ Measured @ 10.8 GHz, ▬✕✕✕▬ Measured @ 12.8 GHz).
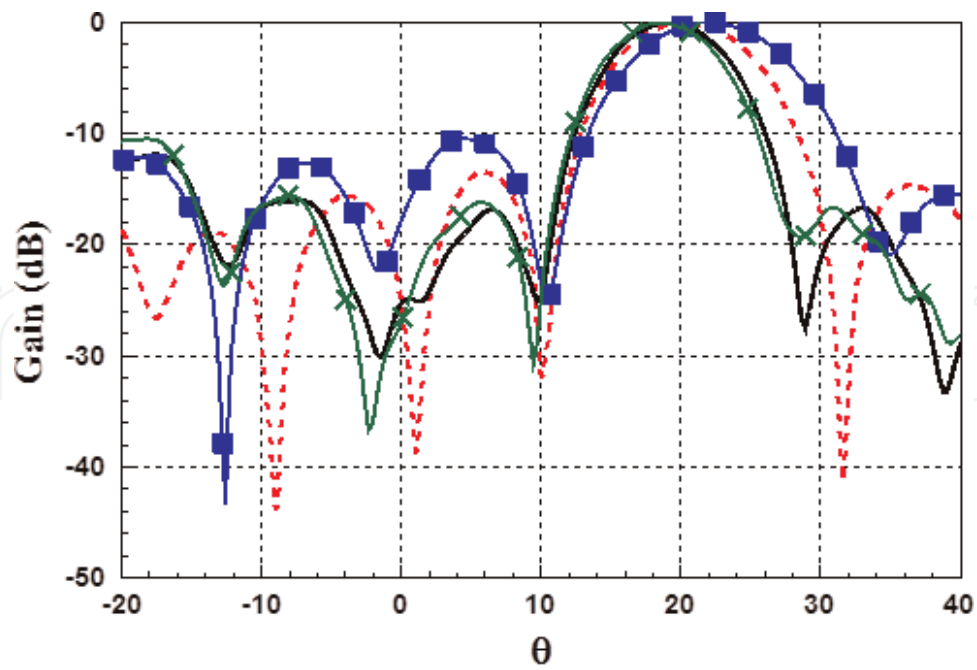
Figure 26. Radiation pattern of vertically polarized full array in φ-plane ($\varphi=0°$ cut) (▬▬▬ Measured @ 11.9 GHz, ▬ ▬ Simulated @ 11.9 GHz, ▬▬▬ Measured @ 10.8 GHz, ✕✕✕✕ Measured @ 12.8 GHz).
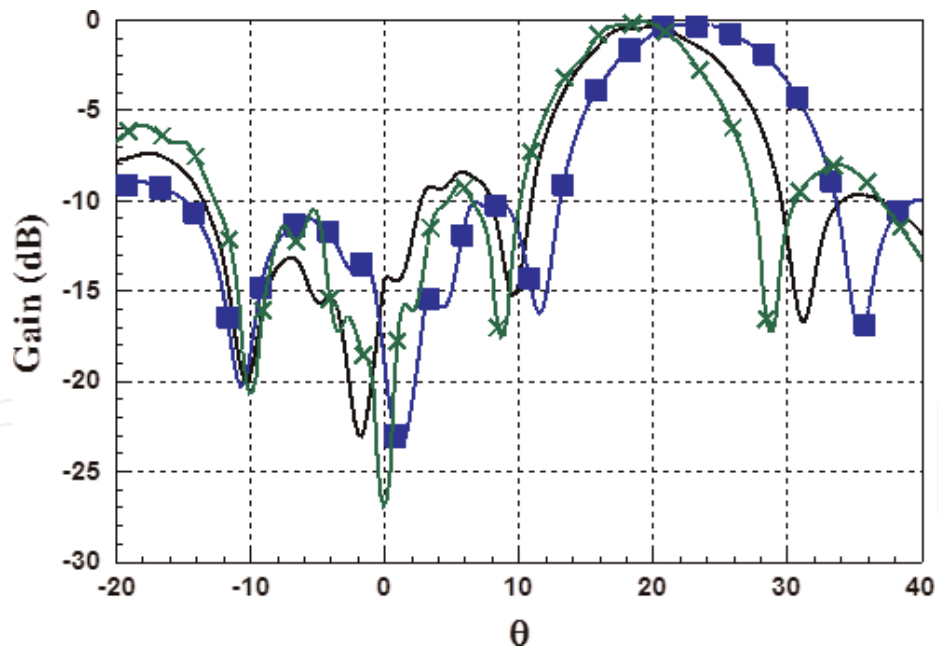

Figure 27. Radiation pattern of horizontally polarized full array in φ-plane ($\varphi=0°$ cut) (▬▬▬ Measured @ 11.9 GHz, ▬▬▬ Measured @ 10.8 GHz, ✕✕✕✕ Measured @ 12.8 GHz).
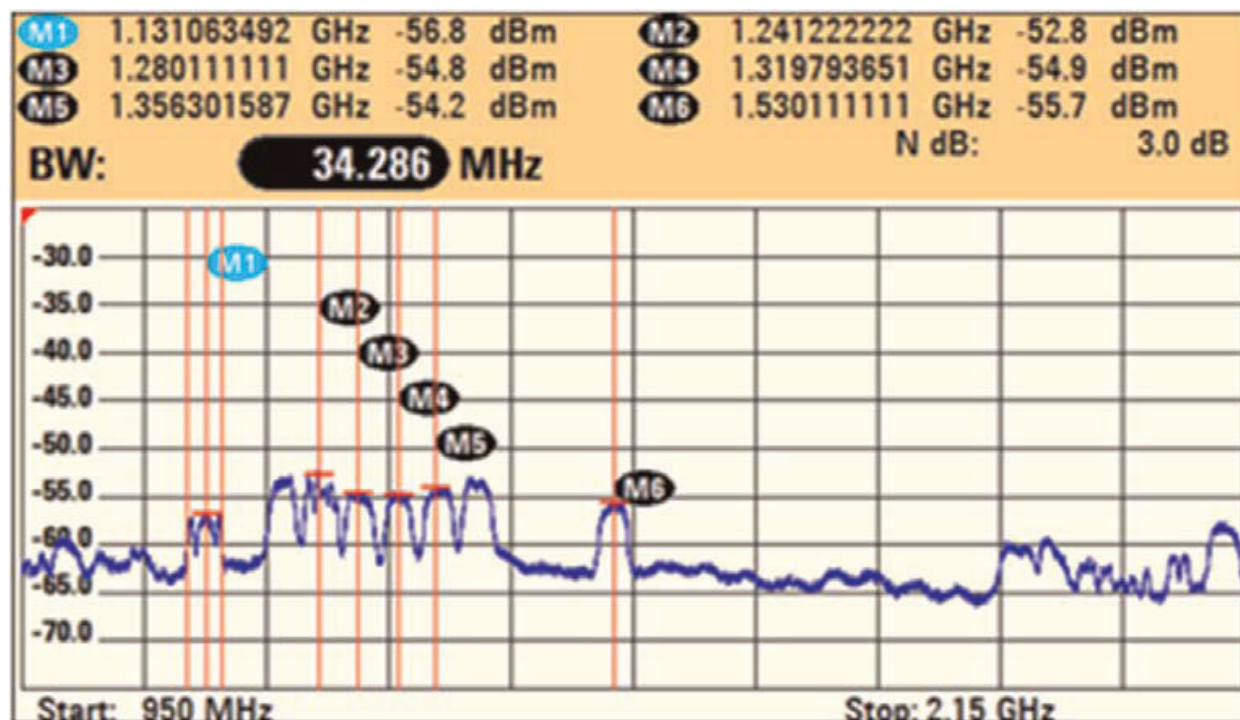
Figure 28. Spectrum analyser measurement of DBS signal.

Author details

Mustafa Murat Bilgic[1]* and Korkut Yegin[2]

*Address all correspondence to: proje@unitest.com.tr

1 Unitest Test and Calibration Services, Istanbul, Turkey

2 Electrical and Electronics Engineering Department, Ege University, Izmir, Turkey

References

[1] Watanabe T., Ogawa M., Nishikawa K., Harada T., Teramoto E., Morita M. Mobile antenna system for direct broadcasting satellite. In: Antennas and Propagation Society International Symposium; 21–26 July 1996; Baltimore, MD, USA. IEEE; 1996. pp. 70–73, vol.1. DOI: 10.1109/APS.1996.549544

[2] Vaccaro S., Tiezzi F., Rúa M., De Oro C. Ku-band low-profile Rx-only and Tx-Rx antennas for mobile satellite communications. In: 2010 IEEE International Symposium on Phased Array Systems and Technology (Array); 12–15 Oct. 2010; Waltham, MA. IEEE; 2010. pp. 536–542. DOI: 10.1109/ARRAY.2010.5613316

[3] Xiang H., Jiang X., Li S. Design of a high gain low sidelobe microstrip antenna array at Ku-band. In: CMC '09 WRI International Conference on Communications and Mobile Computing; 6–8 Jan. 2009; Yunnan. IEEE; 2009. pp. 29–32. DOI: 10.1109/CMC.2009.204

[4] Azdegan R. A Ku-band planar antenna array for mobile satellite TV reception with linear polarization. IEEE Transactions on Antennas and Propagation. 2010; **58** (6):2097–2101. DOI: 10.1109/TAP.2010.2046836

[5] Shahabadi M., Busuioc D., Borji A., Safavi-Naeini S. Low-cost, high-efficiency quasi-planar array of waveguide-fed circularly polarized microstrip antennas. IEEE Transactions on Antennas and Propagation. 2005; **53**(6):2036–2043. DOI: 10.1109/TAP.2005.848510

[6] Kraus J. D., Marhefka R. J. Antennas. 3rd ed. Chapter 2-Basic Antenna Concepts Singapore: McGraw-Hill Education; 2001. 938 p.

[7] McLean J. A re-examination of the fundamental limits on the radiation Q of electrically small antennas. IEEE Transactions on Antennas and Propagation. May 1996; **44**(5). DOI: 10.1109/8.496253

[8] Yaghjian A., Best S. Impedance, bandwidth and Q of antennas. IEEE Transactions on Antennas and Propagation. 2005; **53**(4):1298–1324. DOI: 10.1109/TAP.2005.844443

[9] Pozar D. Microstrip antenna aperture-coupled to a microstripline. Electronics Letters. 1985; **21**(2):49–50. DOI: 10.1049/el:19850034

[10] Kumar G., Ray K. P. Broadband microstrip patch antennas. Chapter 4-Multilayer Broadband MSAs, Artech House; London,United Kindom, 2003. 424 p.

[11] James J. R., Hall P. S. Handbook of Microstrip Antennas: IET; London, United Kindom, 1989. 1312 p.

[12] Targonski S., Waterhouse R., Pozar D. Wideband aperture coupled stacked patch antenna using thick substrates. Electronics Letters. 1996;**32**(21):1941–1942. DOI: 10.1049/el:19961306

[13] Pozar D., Targonski S. Improved coupling for aperture coupled microstrip antennas. Electronics Letters. 1991; **27**(13):1129–1131. DOI: 10.1049/el:19910705

[14] Serra A., Nepa P., Manara G., Tribellini G., Cioci S. A wide-band dual-polarized stacked patch antenna. IEEE Antennas and Wireless Propagation Letters. 2007; **6**:141–143. DOI: 10.1109/LAWP.2007.893101

[15] Rostan F., Gottwald G., Heidrich E. Wideband aperture-coupled microstrip patch array for satellite TV reception. In: Eighth International Conference on Antennas and Propagation; 1993; Edinburgh. IET; pp. 190–193, vol. 1.

[16] Jackson D. R., Alexopoulos N. G. Simple approximate formulas for input resistance, bandwidth, and efficiency of a resonant rectangular patch. IEEE Transactions on Antennas and Propagation. 1991; **39**(3):407–410. DOI: 10.1109/8.76341

[17] Gera A. The radiation resistance of a microstrip element. IEEE Transactions on Antennas and Propagation. 1990; **38**(4):568–570. DOI: 10.1109/8.52277

[18] Pues H., Van de Capelle A. Accurate transmission-line model for the rectangular microstrip antenna. IEE Proceedings in Microwaves, Optics and Antennas. December 1984; **131**(6):334–340. DOI: 10.1049/ip-h-1.1984.0071

[19] Das B., Joshi K. Impedance of a radiating slot in the ground plane of a microstripline. IEEE Transactions on Antennas and Propagation. 1985; **30**(5):922–926. DOI: 10.1109/ TAP.1982.1142922

[20] Edimo M., Mahdjoubi K., Sharaiha A., Terret T. Simple circuit model for coax-fed stacked rectangular microstrip patch antenna. IEE Proceedings—Microwaves, Antennas and Propagation. 1998; **145**(3):268–272. DOI: 10.1049/ip-map:19981853

[21] Choi W., Cho Y. H., Pyo C., Choi J. A high-gain microstrip patch array antenna using a superstrate layer. ETRI Journal. 2003; **25**(5):407–411.

[22] Pirhadi A., Bahrami H., Nasri J. Wideband high directive aperture coupled microstrip antenna design by using a FSS superstrate layer. IEEE Transactions on Antennas and Propagation. 2012; **60**(4):2101–2106. DOI: 10.1109/TAP.2012.2186230

[23] Choi W., Kim J. M., Bae J. H., Pyo C. High gain and broadband microstrip array antenna using combined structure of corporate and series feeding. In: Antennas and Propagation Society International Symposium; 20–25 June 2004; IEEE; 2004. pp. 2484–2487, vol. 3. DOI: 10.1109/APS.2004.1331877

[24] Lee J., Ahn C., Chang K. Broadband circularly polarized aperture-coupled microstrip antenna with dual-offset feedlines. In: IEEE International Symposium on Antennas and Propagation (APSURSI); 3–8 July 2011; Spokane, WA. IEEE; 2011. pp. 1127–1130. DOI: 10.1109/APS.2011.5996481

[25] Mousavi P., et al. A Low-cost ultra low profile phased array system for mobile satellite reception using zero-knowledge beam forming algorithm. IEEE Transactions on Antennas and Propagation. 2008; **56** (12):3667–3679. DOI: 10.1109/TAP.2008.2005928